Polar Climate Instability and Climate Teleconnections from the Arctic to the Midlatitudes and Tropics

GUIDO VETTORETTI, MARC D'ORGEVILLE, AND WILLIAM R. PELTIER

Department of Physics, University of Toronto, Toronto, Ontario, Canada

MAREK STASTNA

Department of Applied Mathematics, University of Waterloo, Waterloo, Ontario, Canada

(Manuscript received 14 February 2008, in final form 12 January 2009)

ABSTRACT

It is generally accepted that the ocean thermohaline circulation plays a key role in polar climate stability and rapid climate change. Recently reported analyses of the impact of anomalous freshwater outflows from the North American continent onto either the North Atlantic or Arctic Oceans demonstrate that, in either case, a clear reduction in the Atlantic meridional overturning circulation, accompanied by an increase in sea ice extent, is predicted. The results also reconcile proxy-inferred Younger Dryas Greenland temperature variations. The aim of the present work is to provide a detailed investigation of the pathways along which the signal associated with overturning circulation anomalies propagates into both the midlatitudes and the tropics and the effect such teleconnections have on the tropical ocean–atmosphere system. The authors consider both the impact of substantial slowing of the overturning circulation due to freshwater forcing of the North Atlantic as well as its recovery after the anomalous forcing has ceased. The changes in tropical climate variability are shown to manifest themselves in shifts of both the typical time scale and intensity of ENSO events in the model. Evidence is presented for mechanisms that involve both atmospheric and oceanic pathways through which such Northern Hemisphere high-latitude events are communicated into both the midlatitudes and the tropics and thereafter transformed into changes in the nature of tropical variability.

1. Introduction

The last glacial-to-interglacial transition was characterized by a sequence of millennial-scale climate regime shifts. One example, the Younger Dryas (YD) cold reversal, occurred at approximately 12.8 kyr (Alley et al. 1993) and lasted for approximately 1.3 kyr. At the end of the YD cold interval, the climate system rapidly returned to full Northern Hemisphere interglacial warmth with Greenland Ice Sheet Project 2 (GISP2) summit annual average temperature rising by approximately 10°C within a period of at most several decades (Grachev and Severinghaus 2005) at the Younger Dryas/Preboreal (YD/PB) transition (11.5 kyr). The question of meltwater routing from the continents to the oceans during the last deglaciation (e.g., Manabe and Stouffer 1997) is critical for our understanding of the way the Atlantic meridional overturning circulation (AMOC) would have been affected.

An especially prominent proposal (Broecker et al. 1989) is that, prior to the onset of the YD, meltwater generated by the retreat of the Laurentide ice sheet was being routed from glacial Lake Agassiz through the Mississippi River system into the Gulf of Mexico. At the onset of the YD, however, this route to the sea was abandoned when continental drainage is hypothesized to have switched to the east through the St. Lawrence River system to the Atlantic. Given the inability to identify the spillway that the eastward flow of meltwater would have occupied (Lowell et al. 2005), it has been suggested that the runoff event that led to YD cooling entered the Arctic Ocean via the Mackenzie River route to the north (Tarasov and Peltier 2005). It has been demonstrated that the impact of Arctic freshening is essentially identical to the impact of Atlantic freshening in so far as the

Corresponding author address: Dr. Guido Vettoretti, University of Toronto, Department of Physics, 60 St. George St., Toronto, ON M5S 1A7, Canada.
E-mail: g.vettoretti@utoronto.ca

DOI: 10.1175/2009JCLI2481.1

impact on the AMOC is concerned (Peltier et al. 2006; Peltier 2007).

While there is evidence for a reduction in the strength of AMOC at Last Glacial Maximum of approximately 40% of the Holocene (or modern) value based upon the protactinium/thorium (Pa/Th) tracer (McManus et al. 2004; Peltier and Solheim 2004), there remains some debate as to whether the reductions in the AMOC led to global climate repercussions (e.g., Barrows et al. 2007; Applegate et al. 2008). Recently, EPICA Community Members et al. (2006) have clearly illustrated the existence of a climate-related temperature connection between the two geographic poles of the planet [e.g., the Antarctic Cold Reversal during the Bølling–Allerød (BA) transition]. New Zealand glacier advance and changes to the surrounding ocean temperature during the YD transition (Barrows et al. 2007) suggest that glacier advance at the time of the YD is not correlated with the onset of cooling in the north, but rather with the warming of the surrounding oceans. This supports the north–south seesaw hypothesis (Broecker 1998; Stocker 1998).

Here we will focus attention on the mechanisms by which the impact of AMOC-related rapid climate change events may be transmitted meridionally into the tropics and zonally to other midlatitude locations. In particular, we will focus upon the impact of changes in AMOC on one of the main modes of interannual global climate variability, the El Niño–Southern Oscillation (ENSO) phenomenon. ENSO, a coupled ocean–atmosphere dynamical process, is characterized by enhanced spectral variability of Pacific sea surface temperatures (SSTs) with a time scale of 2–7 yr (for a recent review of the phenomenon itself, see McPhaden et al. 2006). There exists considerable evidence that ENSO has exhibited markedly different behaviors throughout the recent geologic past.

A recent Holocene reconstruction of ENSO variability using deep sea sediments in the ENSO source region has provided some indication as to how the equatorial Pacific thermocline has evolved (Koutavas et al. 2006). Although this record is not reliable during the YD, it suggests that the recorded ''La Niña–like'' mid-Holocene mean thermocline evolved previously from a more ''El Niño–like'' state (i.e., from an enhanced equatorial Pacific zonal SST gradient during the early Holocene to a weaker gradient during the mid-Holocene). The state of the tropical Pacific during deglaciation remains controversial, with some records showing contradicting results in temperature reconstructions (e.g., Koutavas et al. 2002; Kienast et al. 2006) along with differences in ocean salinity and precipitation (e.g., see Pahnke et al. 2007 for a summary). Two records attempt to provide information on the variation of the strength of ENSO events during and following Last Glacial Maximum: a sediment core located at Laguna Pallcacocha, a small catchment basin that is 4060 m above sea level in the southern Ecuadorian Andes, records Holocene precipitation/runoff events inferred to be associated with a strong El Niño (Rodbell et al. 1999; Moy et al. 2002), and a continuous record of marine sediments from the El Niño region off the coast of Peru provides clear evidence of ENSO variability over the past 20 000 yr (Rein et al. 2005). The sediment record from Peru indicates an increase in the number of intense El Niño events beginning at approximately 18 000 yr before present, with consistently strong events coincident with Heinrich event 1, an event that led to an almost total collapse of the AMOC (McManus et al. 2004). The proxy record of Rein et al. (2005) suggests weaker El Niño events before, and at the onset of, the Younger Dryas (12.8 kyr) but stronger El Niño activity during the latter part of the Younger Dryas. Both the Ecuadorian and Peruvian proxy records suggest a marked reduction in El Niño activity between 8 and 5.5 kyr, which corresponds to the mid-Holocene warm period, with stronger El Niño activity occurring during the second and third millennia before present. Timmermann et al. (2007) argue that the Rein et al. (2005) record may be difficult to interpret, especially as far as separating orbital influences and AMOC influences on ENSO variability is concerned. With the Moy et al. (2002) record stressing millennial-scale ENSO variability and the Rein et al. (2005) record emphasizing multidecadal variability, we are left with the impression that ENSO may well have evolved on many different time scales. For a concise review of reconstructed paleo-ENSO behavior during the last deglaciation the reader is referred to Shulmeister et al. (2006), who suggest that multiple modes contributing to ENSO periodicity may have been active throughout deglaciation.

Reconstructing ENSO activity using sparse data does not necessarily imply that the spatial patterns of tropical Pacific variability that occur on millennial and orbital time scales are consistent with the detailed patterns established on the basis of the high-quality instrumental records of the last two decades (Rosenthal and Broccoli 2004). Thus modeling studies and model-based intercomparisons of paleo-ENSO predictions provide a useful means of investigating possible mechanisms that may contribute to the behavior of this mode of variability under changing boundary conditions (e.g., Timmermann et al. 2007). If fidelity in modeling the variability of ENSO in response to changes of the AMOC can be established for past events, we may then have increased confidence in the projected impact upon this crucial phenomenon in global warming calculations.

Examining ENSO from the perspective of coupled climate model predictions under past, present, and future climate scenarios (Otto-Bliesner 1999; Federov and Philander 2000; Peltier and Solheim 2004) provides a means to assess the fidelity of these predictive models.

Studies of the impact of freshwater forcing on tropical Pacific climate variability (e.g., Zhang and Delworth 2005; Dong and Sutton 2007) have discussed several of the mechanisms that could be involved in supporting an ''atmospheric bridge'' between the polar Atlantic and tropical Pacific Oceans. Timmermann et al. (2005) has suggested that an ''oceanic bridge'' could also be involved in teleconnecting the Atlantic and the tropical Pacific Oceans through the propagation of coastal Kelvin waves. A recent intercomparison study (Timmermann et al. 2007) of the impact of freshwater forcing of the North Atlantic on ENSO variability in five different coupled models found a substantial weakening of the annual cycle in the majority of the simulations and a subsequent increase in ENSO variability. The study demonstrated a clear connection between changes in AMOC strength and tropical Pacific climate variability. Other recent studies have investigated links between the Atlantic multidecadal oscillation (AMO) and Pacific climate variability such as ENSO and the Pacific decadal oscillation (PDO; e.g., Dong et al. 2006; Zhang and Delworth 2007; D'Orgeville and Peltier 2007). Krebs and Timmermann (2007) investigated the global response of an Earth System Model of Intermediate Complexity (EMIC) to reductions in AMOC in fully and partially coupled atmosphere–ocean scenarios. In a recent study, Wu et al. (2008) investigate in detail the teleconnections from the North Atlantic to the tropical Pacific during an AMOC reduction. This study notes a mechanism for the propagation of North Pacific cooling along Baja California into the western tropical Pacific during a freshwater flux (FWF) event.

Our purpose in this paper is to explore the impact of one specific agent of glacial climate change on the ENSO process, namely high-latitude cooling over the North Atlantic caused by an abrupt decrease in the strength of the AMOC as a response to high-latitude surface ocean freshening. In the next section, the model that we will employ in these analyses is briefly described along with the design of the freshwater forcing experiments. The results of our analyses are presented in subsections of section 3 that are ordered as follows: 1) Northern Hemisphere climate changes as a result of the reduced strength of the Atlantic MOC; 2) the mechanisms by which the North Atlantic climate signal is teleconnected into the tropics; 3) the changes in the mean state of the tropics and mechanisms for changes in the ENSO dynamics through the FWF event. The final section of this paper provides a discussion of our results and the conclusions.

2. Model climatology and experimental design

The model used in this study is that of the National Center for Atmospheric Research (NCAR), specifically the Climate System Model, version 1.4 (CSM1.4; Boville and Gent 1998) with improved tropical dynamics (Otto-Bliesner and Brady 2001). It is a fully coupled global atmosphere–ocean–sea ice–land surface model without flux adjustments. The atmospheric component of the model is CCM3.6 (T31L18) with an equivalent grid spacing of $3.75° \times 3.75°$ and 18 vertical levels (Kiehl et al. 1998). The land surface model, LSM1, has specified vegetation types and a comprehensive treatment of surface processes (Boville et al. 2001). The ocean model is the NCAR Ocean Model (NCOM1.4) that has 25 vertical levels, 3.6° longitudinal grid spacing, and latitudinal spacing of 1.8° poleward of 30° that smoothly decreases to 0.9° within 10° of the equator (Gent et al. 1998). The sea ice model (Weatherly et al. 1998) includes ice thermodynamics based on a three-layer model (Semtner 1976) and ice dynamics based on a cavitating fluid rheology (Flato and Hibler 1992). The land model and the sea ice model employ the same grid spacing as the atmosphere and ocean models, respectively. Runoff over land is not treated explicitly in this model, but ocean salinity drift that would therefore be inevitable from incorrect runoff is prevented by instantaneously redistributing the precipitation that falls over land to the ocean by an adjustment of the precipitation field over the ocean.

A series of experiments have been conducted in which freshwater forcing was applied over the ocean surface by adjusting the amount of freshwater the ocean received from the model coupler from 50° to 70°N over the North Atlantic basin. Four experiments were conducted in which the North Atlantic was forced by FWF of 0.1, 0.2, 0.3, and 1.0 Sv ($1 \text{ Sv} \equiv 10^6 \text{ m}^3 \text{ s}^{-1}$) for a period of 100 yr. The experiments include a 200-yr statistically stabilized prehosing control with preindustrial boundary conditions (CO_2 = 280 ppmv; modern orbital parameters, modern land surface). After the forcing interval, the simulations were run for a minimum of 300 yr. The vast majority of the results described in section 3 of this paper focus on the 1.0-Sv experiment and the impact that this freshwater forcing applied to the North Atlantic has on the tropical Pacific.

The nature of the tropical ocean climatology in CSM1.4 has been described in detail by Otto-Bliesner and Brady (2001). They found that the temperature structure of the tropical Pacific thermocline, represented by the depth of the maximum vertical temperature

gradient through the 20°C isotherm, is simulated quite well in the model although the thermocline is insufficiently sharp due in part to the low resolution of the ocean model. In the CSM1.4 model to be employed in the current study, the tropical control climatology is characterized by a salinity distribution in the equatorial Pacific that differs from that which is observed. The global sea surface salinity (SSS) requires about 1500 yr to equilibrate at which point it is more than 2 practical salinity units (psu) below the observed global SSS. This is a result of the salinity drift in the coupled model that occurs when the atmospheric component (CCM3.6) is coupled to the ocean component (NCOM1.4) without flux adjustments. In equilibrium, the tropical surface waters are too fresh while the deep ocean is too saline, resulting in a mean state in which the vertical density gradient is larger than that observed.

Another pertinent issue that should be addressed in the setup of this experiment involves global salinity compensation during the addition of freshwater to the North Atlantic. Many FWF studies (e.g., Stouffer et al. 2006) have not used global salt compensation during the FWF experiments. Global salinity conservation is meant to mimic the effect of holding sea level constant (Stocker et al. 2007) and to remove the impact of salinity changes on the ocean circulation. The FWF experiments in this study do not use global salt compensation. Stocker et al. (2007) conducted a series of experiments using both a global coupled model [Community Climate System Model, version 3 (CCSM3)] and a model of intermediate complexity (ECBilt-CLIO) to investigate changes in salt compensations and eddy-mixing parameterizations during FWF experiments. Their study revealed that the Southern Ocean warms more when global ocean salinity is conserved during the AMOC shutdown as freshwater is added to the North Atlantic.

Another relevant boundary condition in this set of experiments is the state of the Bering Strait. In this model the Bering Strait is closed, which is consistent with the conditions that occurred at the onset of the Younger Dryas event. Hu et al. (2007) investigated the effects of keeping the Bering Strait opened or closed during a FWF event. In a set of FWF experiments using the NCAR CCSM2, Hu et al. (2007) noted that shutdown of the AMOC occurs in a similar manner in both the closed and open Bering Strait experiments but that the recovery was delayed by approximately 100 yr in the closed strait experiment because of reduced transports from the Atlantic into the Pacific via the Arctic Ocean.

Many of the FWF simulations in the literature have used modern boundary conditions, and this has been done in this experiment. The use of glacial boundary conditions in this FWF experiment will need to be address at a later time. In one FWF sensitivity study using CCSM3, Bitz et al. (2007) have previously investigated the recovery of the thermohaline circulation (THC) under Last Glacial Maximum (LGM), modern, and $4 \times CO_2$ stabilized conditions. In each of the different climate regimes the THC is observed to recover in a nontrivial manner, with the recovery occurring fastest with modern conditions, followed by the $4 \times CO_2$ experiment, and then by the LGM experiment. In their study, the LGM THC recovered most slowly because of the expansion of sea ice cover in the North Atlantic, which reduced surface heat loss and increased freshwater supply over the normal sites of North Atlantic Deep Water (NADW) production.

3. Results

The results are organized in the following manner:

- The reduction of the AMOC is discussed first, in order to establish an initial basis on which to understand the dynamical mechanisms and teleconnections.
- The teleconnections are subsequently discussed, first, following the North Atlantic–Caribbean–tropical Pacific pathway, and second, with regard to the effect of large-scale rearrangements of the Northern Hemisphere atmospheric circulation and how these modify the circulation in the Pacific.
- The actual changes in the tropical Pacific, both in the atmospheric circulation and the oceanic waveguide, are considered.

a. Reductions in Atlantic meridional overturning circulation

Records of air temperatures are derived from $\delta^{18}O$ values in ice cores retrieved from Summit, Greenland (e.g., Grachev and Severinghaus 2005), and records of Atlantic Ocean overturning circulation may similarly be recovered from Pa/Th measurements in deep sea sedimentary cores (e.g., McManus et al. 2004). Taken together, these records unequivocally connect reductions in surface air temperature with reductions in AMOC strength during the YD. The maximum of the meridional overturning streamfunction in the Atlantic (not including the surface ocean boundary layer) represents the AMOC at approximately 30°N and 1000-m depth (Fig. 1). Changes in AMOC strength demonstrate the rapid diminution in the overturning strength as the freshwater is applied to the North Atlantic for 100 yr in the 0.3- and 1.0-Sv experiments performed with the CSM1.4 model. The 0.1- and 0.2-Sv experiments yield a smaller response to the addition of freshwater. The 0.1-Sv experiment carried out with this model has one

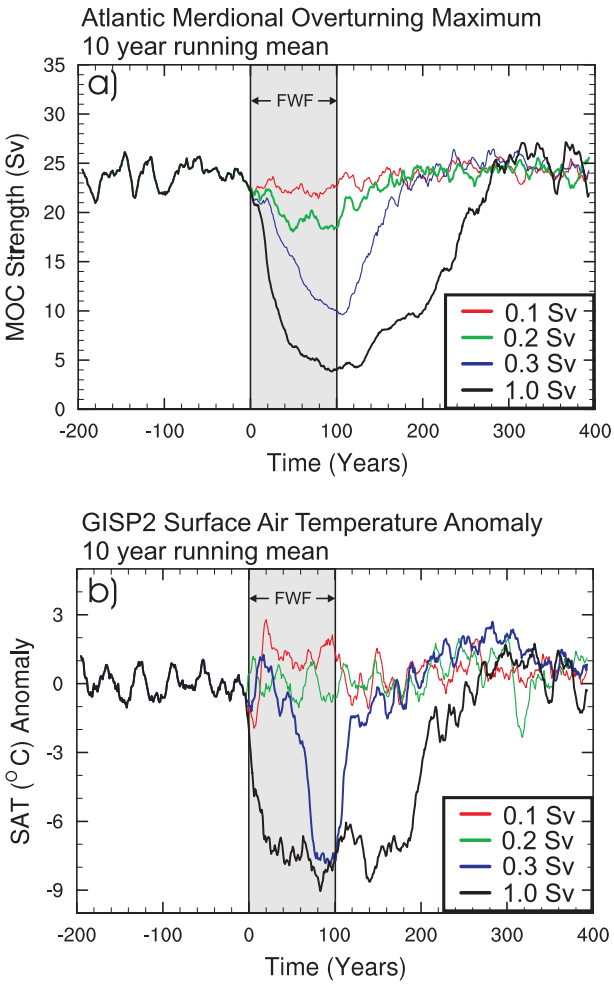

FIG. 1. (a) Time series of the 10-yr running mean Atlantic thermohaline circulation maximum (not including the surface boundary layer) for different forcing experiments and (b) the 10-yr running mean surface temperature anomaly at the Greenland GISP2 location within the model.

of the weakest responses of a set of models that participated in a Coupled Model Intercomparison Project (CMIP) intercomparison of the consequences of freshwater forcing of the North Atlantic (Stouffer et al. 2006). The surface air temperature anomaly response in the coupled model simulation at the GISP2 Greenland ice core location (72.6°N, 38.5°W; Alley et al. 1993) is displayed in Fig. 1b. This anomaly is computed from the temperature time series differenced with the 100-yr average before the onset of the freshwater forcing anomaly. The 0.1- and 0.2-Sv experiments display a similar temperature response, with the 0.1-Sv experiment showing a slight warming during the freshwater forcing. This warming is analogous to a warming that is also observed in other models in the set of CMIP model responses in the Arctic (Stouffer et al. 2006) and is related to a reorganization of the locations of deep-water formation at high latitudes. The surface air temperature response at the GISP2 site in the 0.3- and 1.0-Sv experiments demonstrates the highly nonlinear temperature response of this region to the introduction of freshwater in the North Atlantic. While the 0.3- and 1.0-Sv simulations delivered reductions in overturning circulation strength of 5 and 10 Sv, respectively, from a control of about 23 Sv, they both produce the same GISP2 surface air temperature anomaly of about −8°C, albeit for different durations of time. This simulated temperature anomaly is in close accord with recent inferences by Grachev and Severinghaus (2005; 10°C ± 4°C). The likely explanation for the similar temperature responses in the two more intense FWF experiments lies in the nature of the expansion of sea ice during the model's response to reductions in overturning circulation and the surface freshening of the North Atlantic region, both of which amplify sea ice growth (see also Peltier et al. 2006). This result may reflect the nature of the surface response to a reduction in AMOC and expansion in sea ice past critical threshold values.

A time–latitude plot of March and September sea ice mass along with the annually averaged ocean mixed layer depth for the 1.0-Sv FWF experiment (Fig. 2) illustrates the time evolution of the state of the surface of the central North Atlantic at 30°W from 200 yr before the FWF begins, during the 100 yr of FWF, and then throughout the recovery stage for 500 yr. The sea ice mass is characterized by a larger change in March (Fig. 2a) than in September (Fig. 2b) and reaches latitudes south of 50°N during the FWF period and the following 100 yr after the forcing is turned off. The sea ice retreats beyond the prehosing state during the recovery, but returns to the prehosing state by about 150 yr after the anomalous freshwater input has ceased. The changes in sea ice mass thus appear to be more important during the winter season than in summer and would appear to influence NADW formation during this period. An analysis of the evolution of the annually averaged ocean mixed layer depth (Fig. 2c) provides an approximate picture of the cessation and recovery of the North Atlantic convective activity along a meridional transect. The mixed layer depth can be used as a proxy for the stability of the water column, with a deeper mixed layer being associated with enhanced convective activity and overturning circulation. From Fig. 2 it is apparent that there is still some overturning in the extratropical North Atlantic even though the midlatitude North Atlantic mixed layer stabilizes quickly at the onset of the freshwater input from the eastern to western North Atlantic (not shown). Nevertheless,

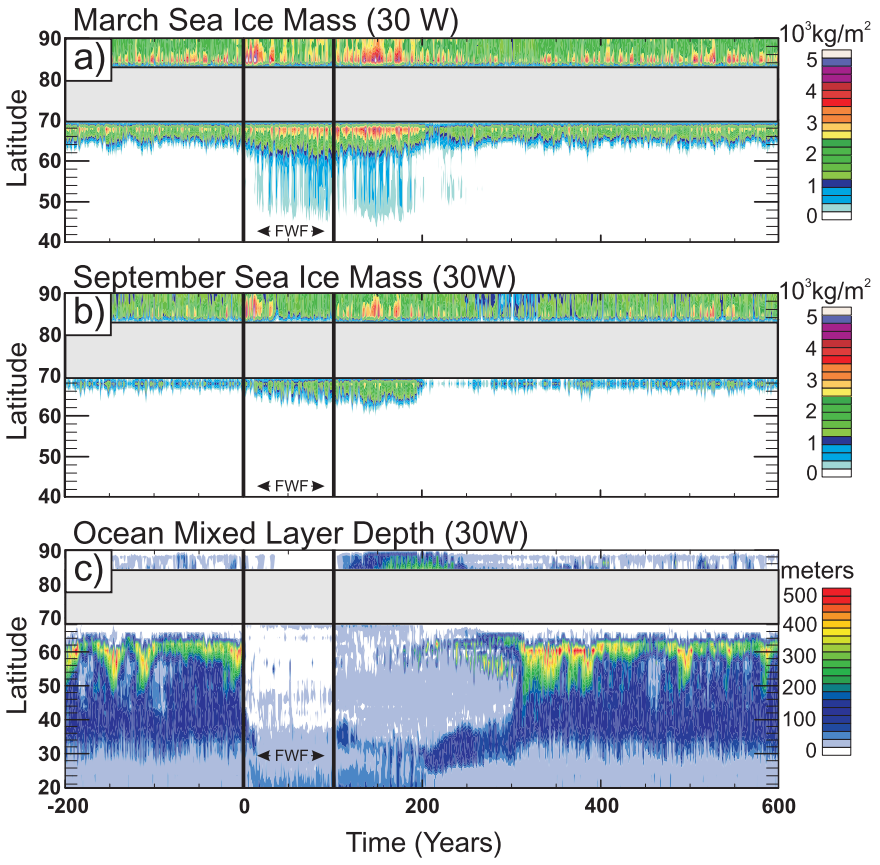

FIG. 2. (a) Latitudinal transects of the March and (b) September sea ice mass and (c) the mixed layer depth in the Atlantic at 30°W. FWF denotes the duration of the freshwater forcing event. Land areas are masked out.

interesting aspects of the changes to the stability of the water column remain visible after the freshwater input stops. The initial recovery of the AMOC starts with convective activity mainly in the Arctic but also at midlatitudes followed by increased activity at about 60°N. The Arctic Ocean temperature profile is characterized by the intrusion of warm waters between approximately 200- and 600-m depth during the freshwater forcing event (see Fig. 8, to be discussed in what follows). This is a result of an inflow of warmer subsurface North Atlantic water into the Arctic during the AMOC reduction. With the cooler Arctic SSTs above, the water column destabilizes (Fig. 2c) during the recovery stage. The state of the mixed layer in the Atlantic returns to its prehosing state 200 yr after the freshwater input ceases, at which time the strength of the overturning circulation (Fig. 1a) has returned to the prehosing level.

Stommel (1961) proposed a salt advection feedback mechanism to affect changes in AMOC. The introduction of freshwater to the North Atlantic would increase stratification and decrease the AMOC, and hence less saltwater would be transported from lower latitudes to higher latitudes. This would allow for the surface of the North Atlantic to be exposed to more freshwater and would further reduce the overturning circulation. In addition to this, the introduction of freshwater to the North Atlantic would not only decrease the AMOC but would also allow more favorable conditions for sea ice formation, namely, reduced SSSs and SSTs. Increasing sea ice extent would further reduce the AMOC and surface temperature in this region by mitigating the air–sea coupling interactions that are critical to deep-water formation. At the same time, the brine release front (and also NADW formation sites) at the edge of the expanding sea ice would move to more southerly latitudes.

The fully coupled model climate evolves in a much more complex manner when compared to the somewhat conceptually rigid conveyor belt model proposed by

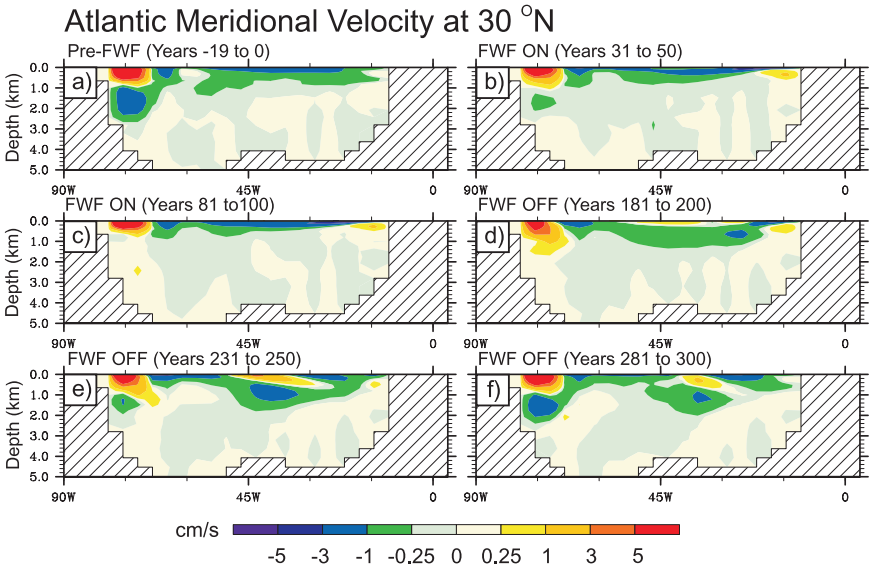

FIG. 3. A longitudinal transect of the Atlantic meridional ocean current velocities at 30°N. (a)–(f) 20-yr time averages of the meridional velocities.

Broecker (1991). The slowdown and recovery of the state of the AMOC may be investigated by studying the temporal evolution of the oceanic meridional velocity along a longitudinal transect of the Atlantic Basin at 30°N (Fig. 3). A number of features in the evolution of the Atlantic Ocean general circulation can be recognized in Fig. 3. Prior to the FWF event (Fig. 3a), the western boundary current is characterized by the strong localized northward transport of warm, saline waters at, and near, the surface (the Gulf Stream) with a deep western boundary current of strong, cold southward flow found between a depth of 1000 and 2500 m. The Atlantic subtropical gyre is characterized by the broad southward transport of cooler water at the surface, ranging over the central and eastern Atlantic. The six panels in Fig. 3 display the evolution of the meridional velocity of the Atlantic from 20 yr before the freshwater forcing to the end of the recovery 200 yr after the 100-yr discharge of freshwater into the North Atlantic has ended. The 20-yr average segments illustrate a number of salient features, in particular 1) the Gulf Stream shallows at the end of the FWF event (Fig. 3c) and then slows down slightly (Fig. 3d) approximately 100 yr after the end of the FWF event. In an EMIC simulation (using ECBilt-Clio) of anomalous freshwater forcing of the North Atlantic, Krebs and Timmermann (2007) demonstrate that decoupling the ocean and atmosphere results in a much longer recovery of the AMOC after shutdown. The wind-driven circulation plays a vital role in the dynamics of the ocean in this coupled atmosphere–ocean simulation and is certainly a dominant factor that supports the eventual recovery of the AMOC in this model. 2) The complete cessation (and slight reversal) of the western boundary return flow at 2000 m in the last 20 yr of the freshwater pulse extends for an additional 100 yr after the FWF stops and explains the majority of the 80% reduction in maximum AMOC strength (Figs. 3c,d and 1a). This cell begins to reform approximately 150 yr after the freshwater input to the North Atlantic has been turned off (Fig. 3e) and recovers to full strength within another 50 yr (Fig. 3f). 3) The top 1000 m of the central Atlantic along the subtropical gyre develops a northward surface flow (Figs. 3d,e) of warm water with a corresponding cold southward transport below, which lasts for approximately 200 yr, or 100 yr after the freshwater forcing has been turned off. This large-scale reorganization clearly alters the heat transport to the North Atlantic, and, since it occurs during the recovery phase of the MOC, it likely impacts the recession of North Atlantic sea ice cover (Figs. 2a,b). In Fig. 2 we see that, after this period of anomalously high northward heat transport in the central and eastern Atlantic, the sea ice actually recedes to northern latitudes, beyond those at which it is observed before freshwater is injected onto the surface of the North Atlantic.

The impact of the freshwater forcing on the behavior of the North Atlantic circulation and the recovery of the AMOC described above provide an initial basis on which to understand the dynamical mechanisms

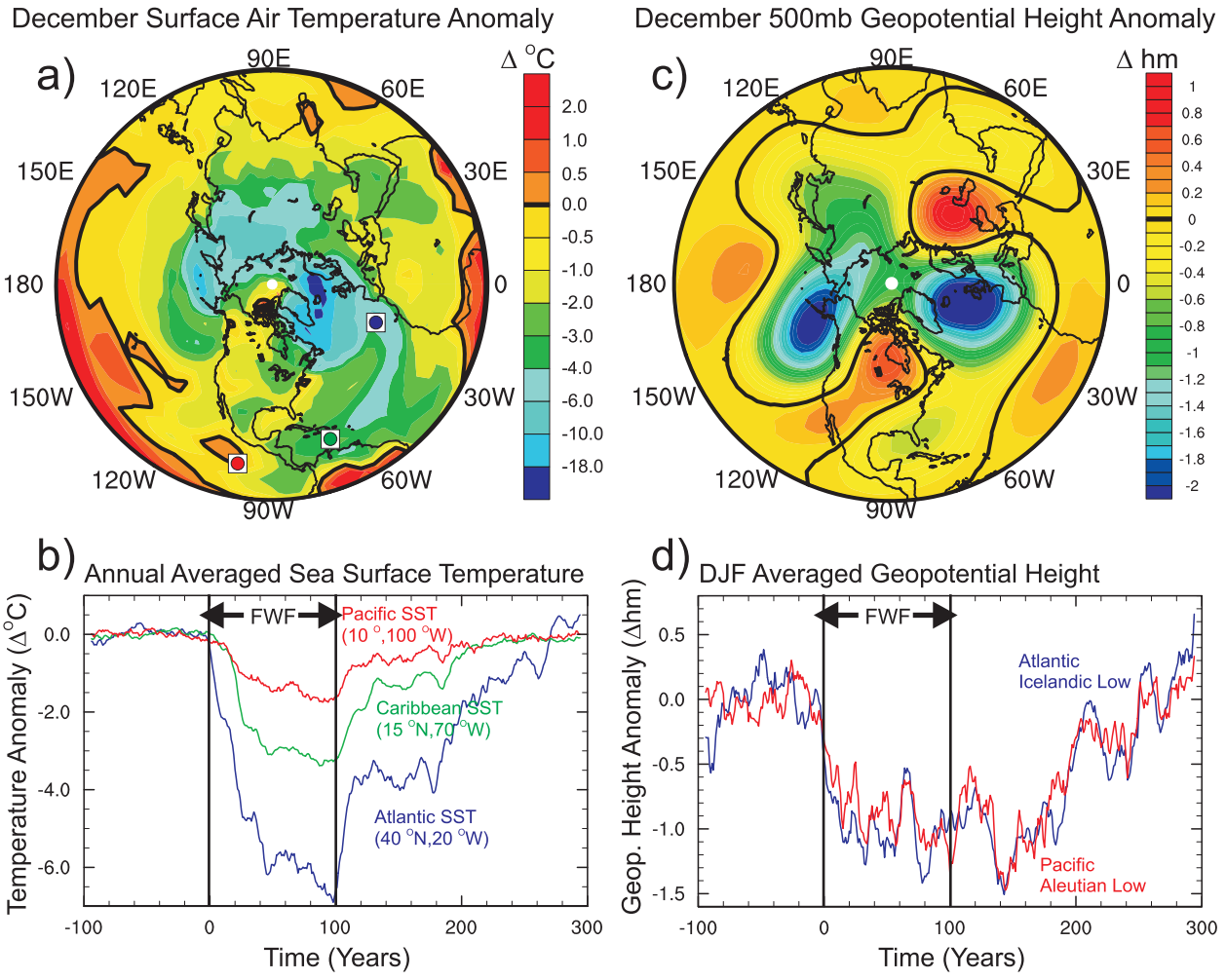

FIG. 4. (a) Average December surface temperature anomaly (years 90–100 of the freshwater forcing minus the control). The red, green, and blue dots represent the locations of the surface 10-yr running mean temperature anomaly time series in (b) the eastern mid-Atlantic, Caribbean Sea, and tropical northeastern Pacific, respectively. (c) The average December geopotential height anomaly (years 90–100 of the freshwater forcing minus the control). (d) The average DJF 10-yr running mean geopotential height anomaly time series of the minima located in the Aleutian low (red line) off of the coast of Alaska and the Icelandic low (blue line) to the east of Greenland. The thick black lines in the contour plot represent the zero line anomalies. FWF denotes the freshwater forcing interval.

involved in teleconnecting the changes in climate from high northern latitudes to the tropics.

b. Atmosphere–ocean teleconnections

The mechanisms involved in the export of climate change at high latitudes to the tropical Pacific have been under investigation for some time (see Liu and Alexander 2007 for a review). They can be classified as meridional mechanisms, which communicate the AMOC signal to the tropical Atlantic, and zonal mechanisms that propagate the AMOC signal to the Pacific through changes in the Walker circulation as well as changes in the large-scale structure of the high-latitude atmosphere. In our FWF simulations, we find that, during the slowdown in the AMOC, the meridional mechanism consists of the transport of cool freshwater from the region of cooling in the North Atlantic, and hence the advection of the cool SSTs by the Atlantic subtropical gyre along the Canary Current to the Gulf of Mexico, the Caribbean Sea, and the tropical Atlantic (e.g., Stocker et al. 2007; Wu et al. 2008). The spatial pattern of this effect can be seen in a plot of Northern Hemisphere average December surface air temperature for the last 10 yr of the freshwater forcing interval (Fig. 4a). This transport reduces Atlantic SSTs north of the equator, while the Atlantic SSTs south of the equator are enhanced. To demonstrate that this cooling signal is efficiently transmitted across the Isthmus of Panama (i.e., the zonal

mechanism) into the equatorial Pacific, three time series of SSTs at point locations in the midlatitude North Atlantic, the Caribbean Sea, and the tropical Pacific are displayed through the onset and recovery of the FWF event (Fig. 4b). The drop in temperature in the midlatitude North Atlantic reaches an annually averaged anomaly of −6°C by the end of the forcing period and then goes through an adjustment process that requires another 200 yr to equilibrate back to mean control values. The negative SST anomalies (SSTAs) in the tropical Pacific are smaller than those in the Caribbean Sea, but they do evolve synchronously, illustrating the operation of an ocean–atmosphere–ocean teleconnection that acts meridionally then zonally. The magnitudes of the SST anomalies in these tropical locations reach maximum amplitude approximately 20 yr into the forcing and then gradually recover by the end of the 100-yr forcing period. The tropical SSTs quickly recover at the end of the FWF period and do not appear to exhibit a large delay with respect to SSTs in the North Atlantic.

A second zonal mechanism, occurring at higher latitudes, can be identified using the December 500-mb geopotential height anomaly (calculated from the average over all Decembers during the final 10 yr of the FWF event). Figure 4c clearly indicates that the stationary planetary wave response induced by the cooling over the North Atlantic has a hemispheric impact with a Northern Hemisphere wavenumber 2 form. In other words, strong negative geopotential height anomalies occur in the region where the December northeastern Pacific Aleutian low minimum resides and in the vicinity of the Icelandic low off the west coast of Greenland (Manabe and Stouffer 1988; Mikolajewicz et al. 1997). The magnitudes of these two anomalous lows are quite variable in strength with significant decadal variability. The boreal winter [December–February (DJF)] geopotential height anomaly time series (Fig. 4d) demonstrates that the anomalous response evolves quickly but takes the entire FWF interval to reach a maximum strengthening of the North Atlantic and North Pacific lows. This results in a surface temperature anomaly that is clearly reflected in the North Pacific surface air temperature anomaly near the coast of Alaska (Fig. 4a). Considering that the Bering Strait is closed in this experiment, this mid–high-latitude zonal ocean–atmosphere–ocean teleconnection is expected to be the dominant influence on the state of the Northern Pacific atmosphere and ocean. It is entirely possible that other atmospheric teleconnections are in operation (e.g., impacts from changes in the northern annular mode; Wu et al. 2008) or that an oceanic teleconnection may operate in which the oceanic FWF signal would be carried from the North Atlantic through an open Bering Strait to the North Pacific (Okumura et al. 2009). The investigation of these mechanisms is however, beyond the scope of this study. In the two subsections that follow, attention is given to the detailed mechanisms involved in these two ocean–atmosphere–ocean pathways.

1) TELECONNECTION TO THE TROPICS

The purpose of this section is to demonstrate the linkage between changes in the North Atlantic and the changes in the tropical Pacific. Since the oceanic mechanism involved in the transport of the cool SST anomaly meridionally into the tropical Atlantic has been discussed, it is useful to examine the air–sea interaction in the meridional and zonal direction with particular focus on the tropics. The upper- and lower-level global atmospheric circulation patterns are displayed by comparing the streamfunction and velocity potential in boreal winter (DJF) and boreal summer [June–August (JJA)]. The rotational and divergent winds that are diagnosed from the streamfunction and velocity potential provide information about horizontal and vertical mass transport. In the control simulation, the streamfunction indicates that there are strong tropical westerly winds at upper levels (Figs. 5a,b) and tropical easterly winds near the surface (Figs. 5c,d). The simulated velocity potential in the control simulation, which is contoured over the streamfunction, is characterized by convergence at 850 mb in the northwest and southwest Pacific warm pool in JJA and DJF, respectively. Likewise, divergence occurs over the Americas and Atlantic at lower levels. The atmosphere flows from regions of negative velocity potential to regions of positive velocity potential. At upper levels the divergence and convergence patterns are reversed. The velocity potential in Figs. 5a–d corresponds with the tropical Walker circulation in the control simulation.

The surface easterlies in the tropical Atlantic that mainly originate from the subtropical North Atlantic high pressure system in DJF and the subtropical South Atlantic high pressure system in JJA provide a conduit to transport the cool SST signal from the Caribbean to the tropical eastern Pacific (Figs. 5c,d). The pressure gradient along the tropical Pacific drives the mean surface easterlies and determines the resultant mean thermocline state, with warm waters building in the western Pacific and cool upwelling surface waters in the eastern Pacific. Changes in the mean Walker circulation, which are a vital component of ENSO dynamics, should therefore play a dominant role in determining mean changes of the Pacific equatorial thermocline and equatorial Pacific oceanic waveguide.

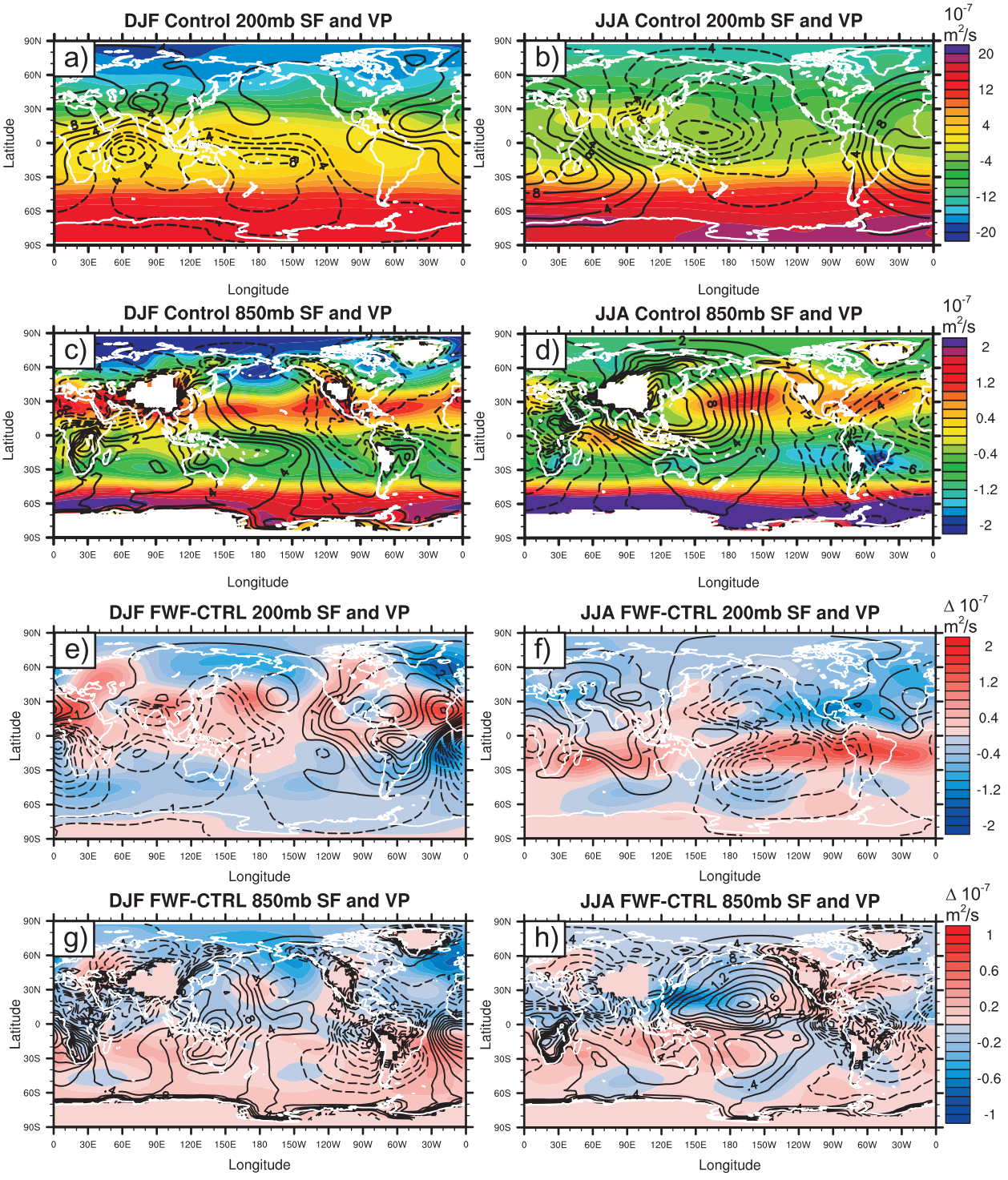

FIG. 5. The average horizontal streamfunction and velocity potential at an upper level (200 mb) and a lower level (850 mb) for winter (DJF) and summer (JJA) for the last 50 yr before the freshwater forcing event begins. (e)–(h) The anomalies (years 50–100 of the freshwater forcing minus the control) for the horizontal streamfunction and velocity potential at upper levels (200 mb) and lower level (850 mb) for winter (DJF) and summer (JJA).

In winter, the 200-mb streamfunction anomalies (Fig. 5e) indicate that the Northern Hemisphere midlatitude jet streams have intensified substantially over the North Atlantic and northwestern Pacific. Much of the intensification and change in orientation of the winds is likely due to the effect of the expanded sea ice edge in high northern latitudes. At 45°N, the transient eddy latent and sensible heat fluxes have increased by approximately 30% (not shown) and indicate that the baroclinicity of the Northern Hemisphere has increased substantially during winter (e.g., see Bush 2003). A large tropical 200-mb streamfunction anomaly in summer (Fig. 5f) demonstrates atmospheric mass flux compensation and a teleconnection between the equatorial Pacific and the equatorial Atlantic through an increase in the upper-level tropical westerlies in summer. Near the surface, the anomalies in the summer 850-mb streamfunction (Fig. 5h) are characterized by a quadrupole streamfunction pattern that spans the western Pacific to the Americas. The net effect of this anomaly during the FWF event is to transmit the cooling signal from the tropical Atlantic into the eastern tropical Pacific and to cause anomalous mean westerlies in the western Pacific during summer. This pattern of two cyclonic anomalies in the western Pacific resembles the Gill (1980) steady-state solution to symmetric heating about the equator. In Fig. 4a, the anomalous Southern Hemisphere heating pattern that results form the reduced AMOC spans north of the equator in the western Pacific during the FWF event and correlates well with the forcing used in the Gill (1980) solution with symmetric heating. In winter, the 850-mb streamfunction anomaly is characterized by a dipole pattern that spans the equatorial Atlantic (Fig. 5g).

In summer in the Northern Hemisphere Atlantic, the subtropical high appears also to be related to the enhanced ridging over North America; a consequence of the enhanced depressions in the Aleutian low and North Atlantic FWF region (Figs. 5d,h). There may thus be a feedback mechanism that operates during the summer in the initial few decades at the start of the FWF event. Northeasterly trades increase in response to an increasing subtropical Atlantic high and drive stronger atmospheric transport into the eastern Pacific over the initial period of freshwater forcing. Previous studies have noted an increase in Northern Hemisphere trade winds (e.g., Zhang and Delworth 2005) and a large anomalous anticyclonic surface circulation in the extratropical Atlantic, which is a consistent feature in a set of atmosphere–ocean coupled general circulation models (AOGCMs) used in an intercomparison study of the impact of FWF on ENSO (Timmermann et al. 2007). Many of these ideas extend to the interaction of the northeasterly trades and the Atlantic and Pacific meridional modes (Chiang and Vimont 2004).

A similar effect, but with an opposite sense, can be seen in the South Atlantic in DJF and JJA, with a weakening of the north and south subtropical anticyclones and an increase of the SSTs south of the equator (Fig. 4a). This may be due to the weakening of the downward branch of the DJF Atlantic Hadley cell located at approximately 30°S. The weakening of the streamfunction will result in a reduction of the transport of cooler SSTs from southern latitudes because of a reduction in the wind-driven circulation and a subsequent reduction in the Benguela Current in the South Atlantic subtropical gyre. This reduction has the effect of increasing the SSTs along the western coast of South Africa by 4°C during the FWF event (not shown) and increasing the equatorial meridional temperature asymmetry. Through air–sea interaction, the positive SST anomaly that persists in September–November (SON) and DJF across the equatorial Atlantic is advected to the eastern tropical Pacific by the Atlantic trade winds during the FWF event in austral summer (DJF). Again through air–sea interaction, the SSTs are subsequently modified in the eastern Pacific, impacting the annual cycle in this region.

The changes in velocity potential between the upper and lower levels during the FWF experiment illustrate mass conservation in the tropics and provide a clearer view of the changes in tropical circulation patterns (Figs. 5e,f). In boreal winter (DJF) at lower levels (Fig. 5g), there is an intensification of the divergent wind over the Americas during the FWF event and increased convergence over the western warm pool. In boreal summer (JJA) at lower levels (Fig. 5h), two approximately symmetric regions of strong convergence form over the central Pacific between approximately 20°N and 20°S. Regions of increased divergence occur over the Indian Ocean and over tropical South America, with the opposite changes occurring at upper levels (Figs. 5f,h). From this analysis, we see that the Pacific Walker cell shifts westward in DJF and eastward in JJA. Whether the Walker circulation intensifies during the FWF event will be the subject of further analysis in what follows.

The divergent wind and vertical pressure velocity from the model are employed to assess changes in the Walker and Hadley circulations during the FWF experiment following Wang (2002). Wang (2002) used the National Centers for Environmental Prediction (NCEP)–NCAR reanalysis from the last half of the twentieth century to illustrate anomalous circulations in the Pacific Walker and Hadley circulation during warm and cold phases of ENSO. Figure 6a displays the divergent

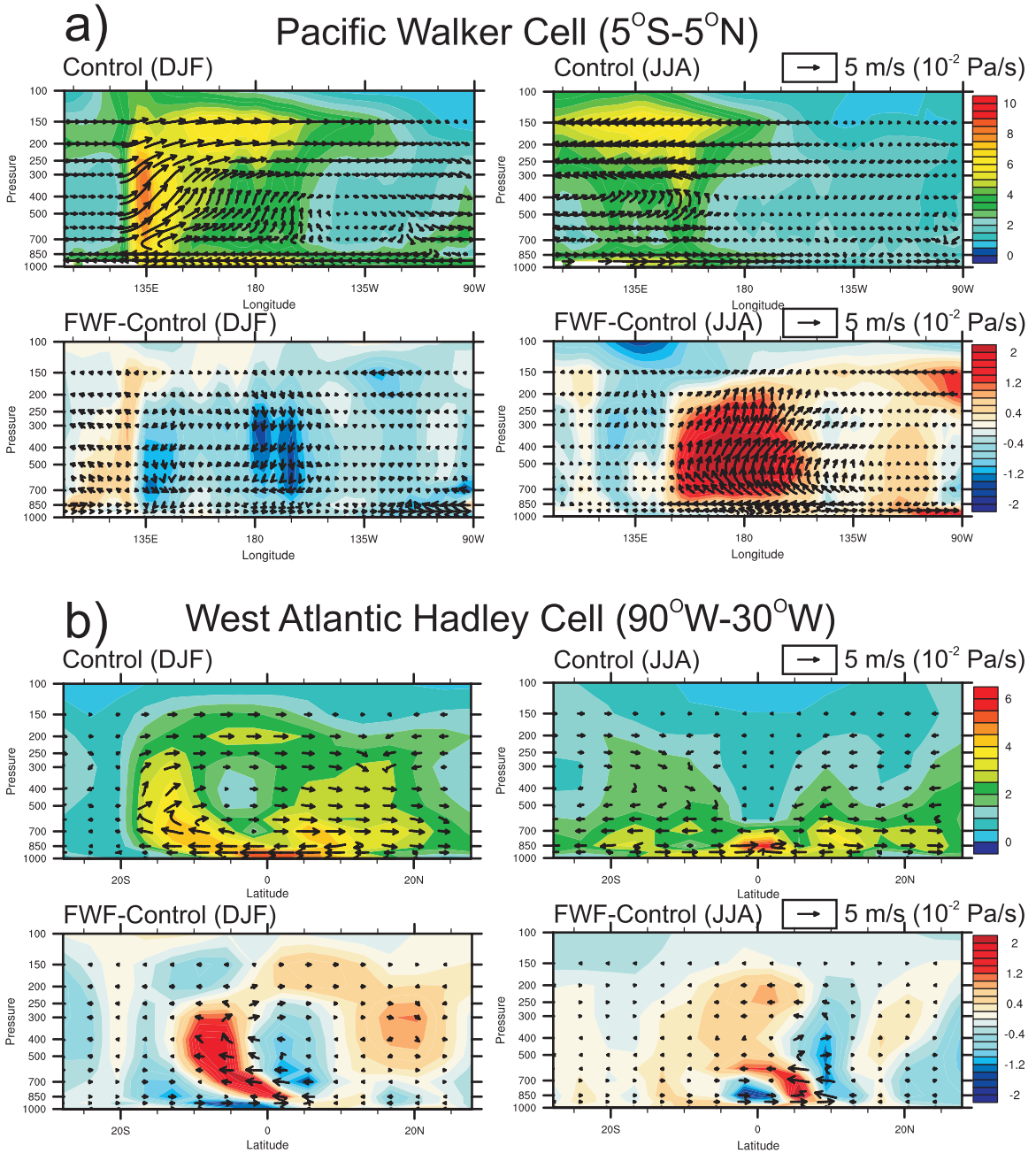

FIG. 6. (a) The Pacific Walker circulation for DJF and JJA. The zonal–vertical control and anomalous (FWF control) circulation is obtained by averaging the divergent wind (m s^{-1}) and vertical pressure velocity (10^{-2} Pa s^{-1}) from 5°S to 5°N. (b) The Atlantic Hadley circulation: the meridional–vertical control and anomalous (FWF control) circulation is obtained by averaging the divergent and vertical pressure velocity from 90° to 30°W. The (c) east and (d) west Pacific Hadley circulation for DJF and JJA. The meridional–vertical circulation is obtained by averaging the divergent wind (m s^{-1}) and vertical pressure velocity (10^{-2} Pa s^{-1}) from 150° to 100°W in (c) and from 120° to 170°E in (d). The FWF anomalies are calculated by subtracting the average of the last 50 yr of FWF from the control. The contouring displays the magnitude of the zonal–vertical or meridional–vertical wind in 10^{-2} $Pa^{1/2}$ $m^{1/2}$ s^{-1}.

wind spatially averaged from 5°S to 5°N across the equatorial Pacific and temporally averaged over the 50-yr period before the FWF event for DJF and JJA. Figure 6a also displays the anomalies between the last 50 yr of the FWF event and the control simulation for boreal winter and summer. The DJF circulation in Fig. 6a is more characteristic of the typical Walker cell than in JJA with ascending motion over the western Pacific

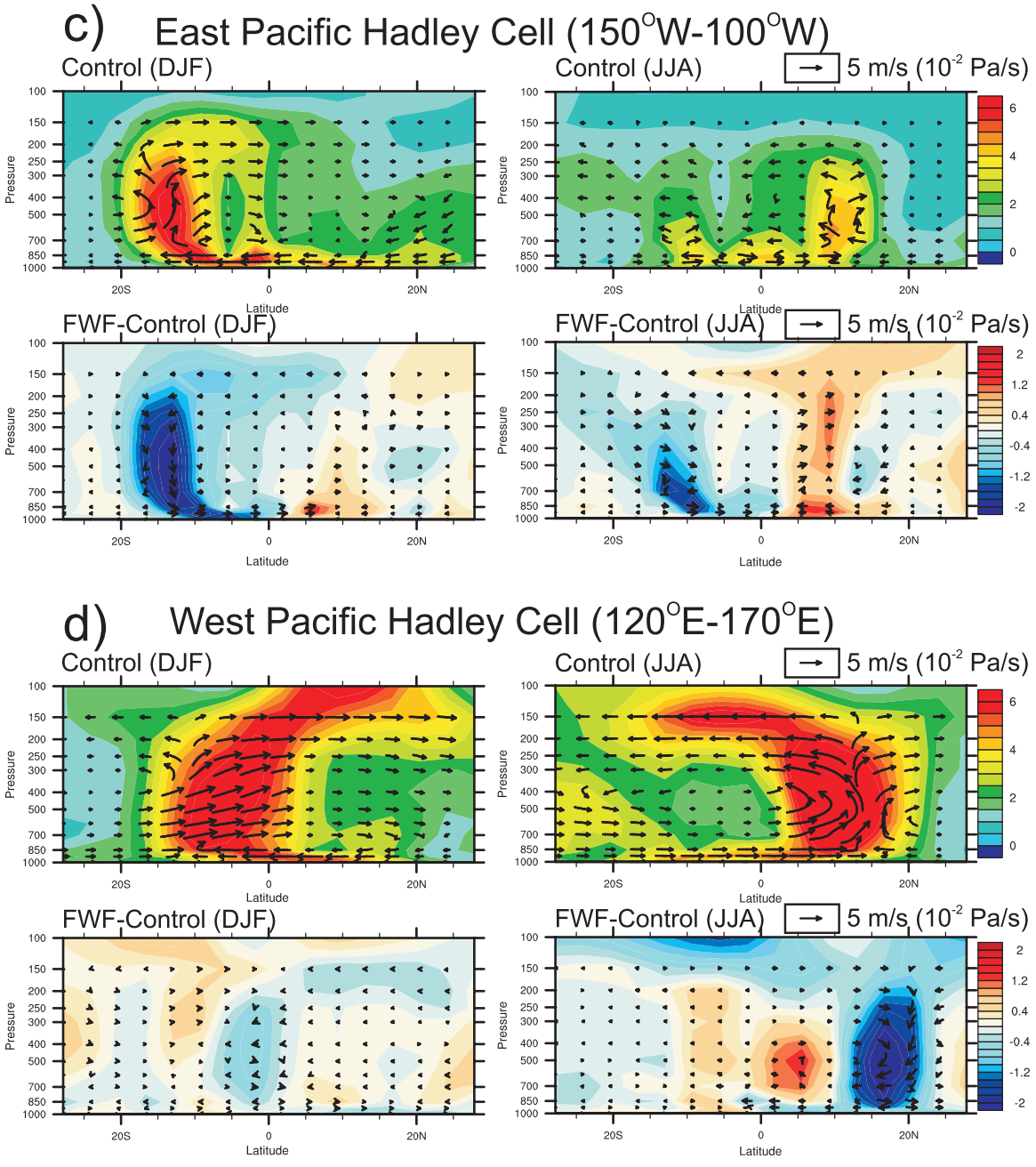

FIG. 6. (*Continued*)

and predominant easterlies at low levels. In JJA, the Walker cell is not as well defined and may be a result of the circulation cell being displaced north of the equator in the model. The anomalies in DJF and JJA display opposite configurations, with reduced ascending (descending) motion in DJF (JJA) over much of the tropical central Pacific. In DJF the Walker circulation appears to shift westward over Indonesia and weaken slightly, whereas in JJA the Walker circulation appears to shift eastward to the central Pacific and strengthen significantly. Thus, the changes in the Walker circulation during the FWF event reflect a seasonal asymmetry.

Figure 6b–d displays the meridional–vertical circulation in the tropical Atlantic and eastern and western Pacific in a similar fashion to the Walker cell displayed in Fig. 6a. In the western Atlantic, the DJF Hadley cell

(Fig. 6b), which has the ascending branch south of the equator, appears to shift northward during the FWF event. Likewise, in JJA, the weaker Hadley cell appears to shift north, slightly contrary to changes expected from a shift in the ITCZ. In the eastern Pacific (Fig. 6c), the ascending branches of the Hadley cell, which are north and south of the equator in JJA and DJF, respectively, change markedly. In DJF the ascending branch of the Hadley cell south of the equator in the eastern Pacific weakens markedly, while in JJA the northern branch intensifies, contrary to the circulation that would be expected in response to the meridionally asymmetric SST mode that forms in the tropical Pacific during the FWF event. In the western Pacific, the strong Hadley cell has a consistent southward shift in both seasons (Fig. 6d). This is consistent with a shift in the ITCZ to the warmer hemisphere.

2) Teleconnection to the midlatitude Pacific

The purpose of this next section is to demonstrate the linkage between changes in the North Atlantic AMOC and the extratropical–North Pacific as illustrated by the increased strength of the geopotential height anomaly in the North Pacific at 140°W (Fig. 4a). Proxy records from Ocean Drilling Project (ODP) site 893A have demonstrated a possible synchronicity in the YD transition between Greenland and the California margin. Hendy et al. (2002), employing a new age model for the upper portion of ODP 893A, have demonstrated a strong correlation between rapid climate changes in Greenland ice cores and marine isotopic records in the Santa Barbara Basin (34.15°N and 120°W) during the last deglaciation. Hendy et al. (2004) show that the California Margin is characterized by increased productivity leading into the YD followed by reduced productivity during the YD. These conditions revert back to the conditions prevalent during the BA transition after the termination of the YD event.

The spring and summer northwesterlies along the coast of California are primarily driven by an anticyclonic circulation present in the midlatitude Pacific and result in Ekman-pumping-induced coastal upwelling and increased net primary productivity in this region. In the FWF experiment, the spatial and temporal strengthening of the Aleutian low during winter can be seen in the mean January sea level pressure and 850-mb winds (Fig. 7a). The stationary wave response from the reduced temperatures (Figs. 4c,d) in the North Atlantic region during the FWF event strengthens the Aleutian low in winter.

A time series of the January alongshore wind velocity as a function of model simulation year at the location of the Santa Barbara Basin reveals a substantial change through the FWF event (Fig. 7b). The variability in winter is much stronger than in summer (not shown) and correlates with the fact the planetary wave response is strongest in winter and thus modifies the winter northeast Pacific circulation. The enhanced difference in Ekman-pumping-induced downwelling over the Santa Barbara Basin during the FWF event occurs as a strengthened southeasterly wind that enters the strong southward geostrophic branch of the Aleutian low and builds throughout the 100-yr period of FWF. The January wind anomaly requires approximately an additional 100 yr to dissipate after the FWF has ceased (Fig. 7b). The wind anomaly implies a local weakening of the Ekman-pumping-forced upwelling in the winter as the climate system along the California Margin adjusts to the high-latitude forcing. While there is no significant change in upwelling in spring and summer during the FWF event, it is possible that the changes in winter will impact the mean annual ocean circulation in this region on longer time scales and therefore have an impact on the spring maximum in primary productivity. Additional analyses are required to assess the details of the mechanisms involved in this teleconnection under a reduced AMOC glacial climate regime (including topographic and ice–albedo forcing), a regime that is not included in this study.

The changes observed in the proxy records connecting changes in the North Atlantic and the North Pacific basin raise the question of whether this atmospherically forced signal between the ocean basins can be propagated to the tropical Pacific through a meridional ocean bridge. Temperature anomalies have been observed to subduct from midlatitudes toward lower latitudes along the outcropping oceanic pycnocline in subsurface oceanic records of the North Pacific during the past several decades (e.g., Deser et al. 1996). There have also been several mechanisms proposed for the transport of water properties from the extratropical Pacific to the tropical Pacific. Gu and Philander (1997) suggested a cycle with an interdecadal time scale that couples the subduction of extratropical ocean temperature anomalies into the tropical Pacific thermocline. With a warming (cooling) of the tropics, the extratropical westerlies increase (decrease) and as a result extract more (less) heat from the extratropical ocean, which then cools (warms) the extratropics. The extratropical temperature anomalies are then subducted into the tropical thermocline where the cycle is repeated.

The latitudinal transect of the annual average potential temperature anomalies across the Pacific (Figs. 8a–c) for years 40–50 of the FWF event illustrates the way in which the cooling signal in the northeastern Pacific SSTs

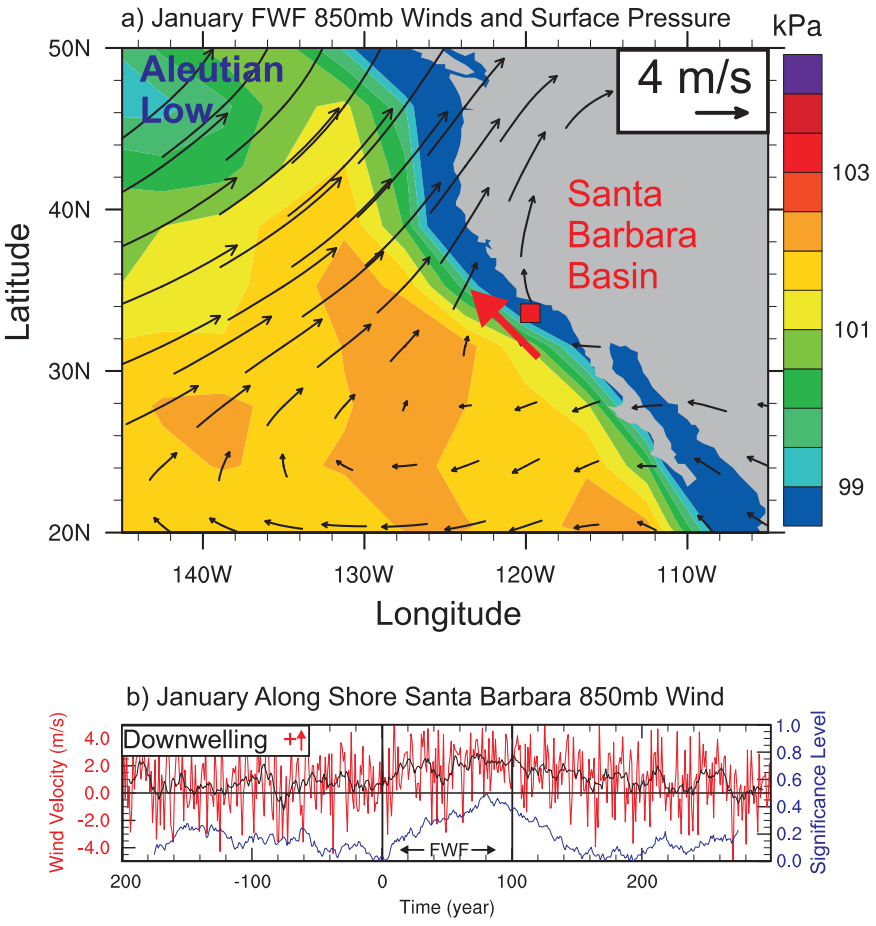

FIG. 7. (a) January average 850-mb winds and surface pressure around the California Margin (years 50–100 of the freshwater forcing event). (b) The time series of the alongshore wind in the direction of the red arrow off of the California Margin is displayed by the red curve in m s^{-1}. The black curve is the 10-yr running mean of the wind speed. The blue curve is a measure of the significance level of the deviation of the 50-yr running mean wind compared with the 200-yr pre-freshwater-forcing average (years −200 to 0) using a standard error function technique. Northeasterly winds during the freshwater forcing event are associated with Ekman-forcing-induced downwelling.

evolves into the subsurface. It appears that the North Pacific temperature signal is separated from the tropics as evidenced by the temperature anomalies in Figs. 8a,b, which appear to propagate subsurface to approximately 30°N. At this point we cannot rule out that modulations in ENSO on a decadal time scale may be impacted by changes induced in the northeastern Pacific through the action of this ocean–atmosphere–ocean bridge.

The novel structure that is observed in the latitudinal transect in the western Pacific (Figs. 8a), the central Pacific (Figs. 8b), and the eastern Pacific (Figs. 8c) at mid–low latitudes during the FWF event may in fact be a result of the reorganization of the tropical Pacific atmospheric circulation. The cool temperature anomaly observed at approximately 20°S and the warm temperature anomaly at approximately 20°N are visible in the entire tropical Pacific (Figs. 8a–c). The fact that this anomaly also exists in the extratropical Atlantic (not shown), and is delayed by approximately 20 yr after the FWF event begins, suggests that this is a result of the reorganization of the atmospheric forcing in response to changes in ocean circulation. The hemispheric anomalies, characterized by downwelling and upwelling motion in the North Pacific and South Pacific, respectively, result from the action of Ekman-pumping-induced by surface wind forcing. A shift in the ITCZ, the subtropical highs, and subtropical ocean gyres redistribute the surface wind stress forcing (equatorward in the

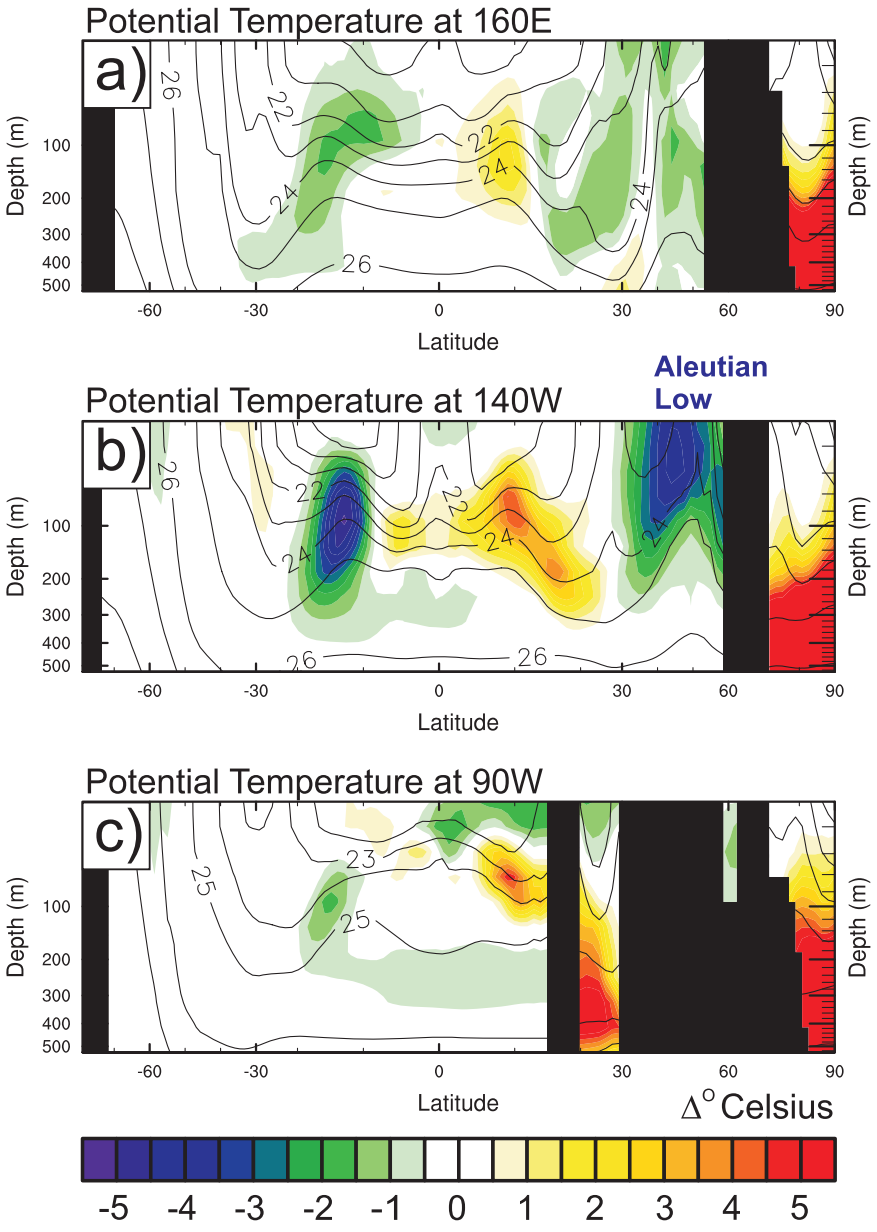

FIG. 8. Latitudinal transects of the annual average potential temperature in the top 500 m of the (a) western, (b) central, and (c) eastern Pacific. The contours of the density isopycnals are plotted in units of (1000 –density) kg m^{-3} (black contours). Ocean bathymetry is masked out in black.

Northern Hemisphere and poleward in the Southern Hemisphere on average).

c. *Tropical Pacific climate variability and ENSO evolution in response to a collapse of the AMOC*

The Niño-3.4 SST index (5°S–5°N, 120°–170°W) from 1870 to 2000 (Fig. 9a) and the corresponding Morlet wavelet power spectrum (Fig. 9b; Torrence and Compo 1998) are obtained from the Hadley Centre Sea Ice and Sea Surface Temperature (HadISST) dataset (Rayner et al. 2003). This scale-independent spectral method is especially well suited to nonstationary time series analysis and demonstrates that much of the observed ENSO power is concentrated in the 2–7-yr power band. From 1870 to 1910 and from 1960 to the present,

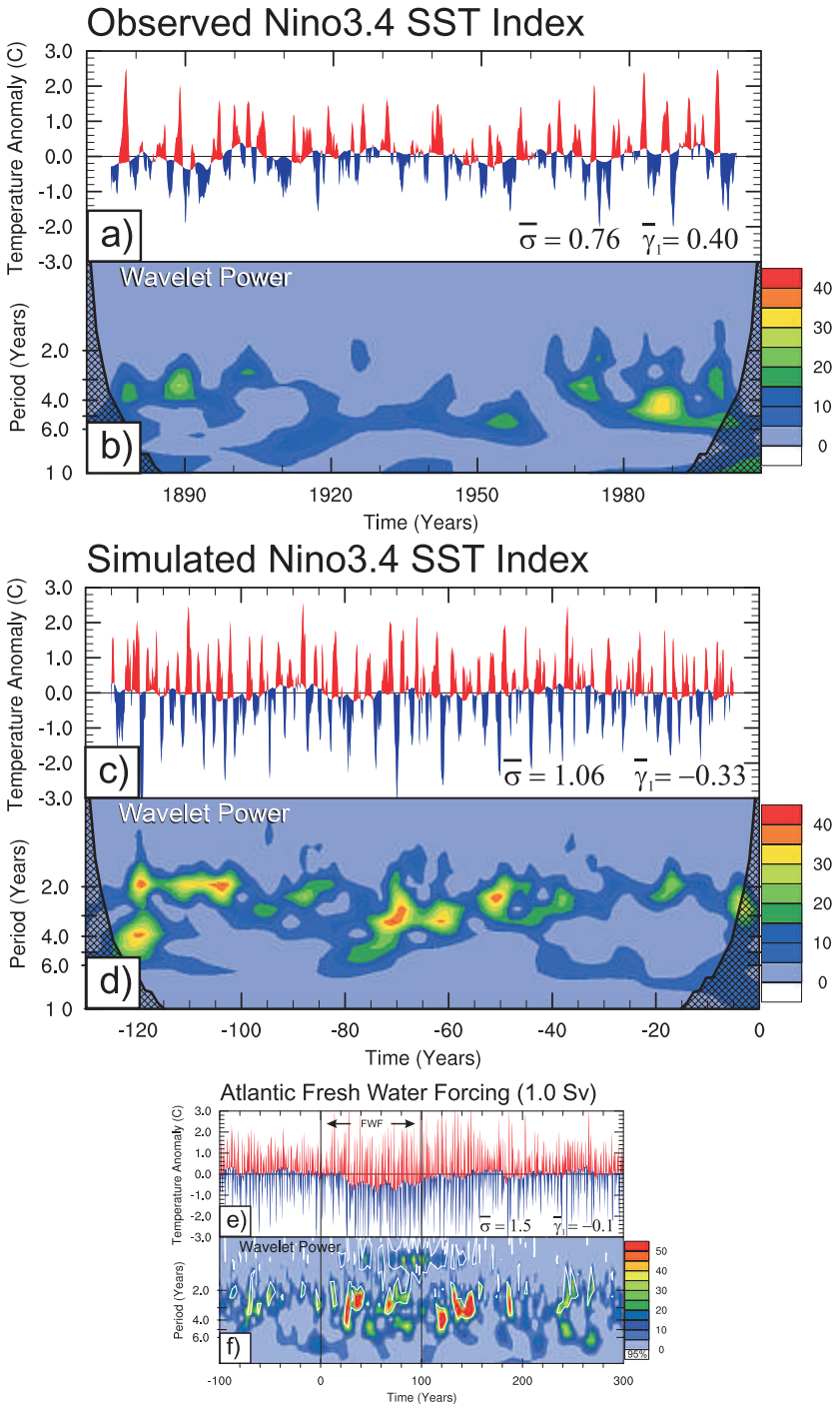

FIG. 9. (a) The 3-month smoothed time series of the Niño-3.4 SSTA index from observations (1870–present). (b) The Morlet wavelet spectrum of the observed Niño-3.4 SSTA index. (c) The simulated preindustrial Niño-3.4 SSTA index and (d) Morlet wavelet spectrum for the 130 yr before the freshwater forcing is applied to the Atlantic. The std dev and skewness of the time series are listed in the bottom right corners of (a) and (c). The positive and negative anomalies in the time series of the observed and simulated Niño-3.4 index are plotted upon a 10-yr running mean. (e) The 3-month smoothed time series of the Niño-3.4 SSTA index from the freshwater forcing experiment (1-Sv experiment). (f) The Morlet wavelet spectrum of the FWF Niño-3.4 SSTA index time series. White contours denote regions that are statistically significant above the 95% confidence level.

observed ENSO variability has been characterized by increased ENSO power in the 2–4-yr band. The observations also have a fairly uniform distribution of power in the 4–8-yr band from 1870 to the present. The model-simulated Niño-3.4 SST index (Fig. 9c) and the ENSO wavelet power spectrum for the control climate (Fig. 9d) is characterized by much greater variability in the 2–4-yr band when compared to observations. Furthermore, the entire time series is lacking significant power in the 4–8-yr band. This feature is a common problem in many modern AOGCMs (Guilyardi 2006) and is likely due to a number of problems (e.g., resolution, cloud and convective parameterizations, etc.). One recent study notes a marked improvement in tropical dynamics when an improved cumulus convective parameterization is added to the model used in this study (Wu et al. 2007).

A time series of the 1-Sv Niño-3.4 SST index (Fig. 9e) reveals large-amplitude El Niño and La Niña events during and after the 100-yr period during which the freshwater forcing is applied. The mean Niño-3.4 SST anomaly is plotted as a departure from a 10-yr running mean. This temperature anomaly decreases by approximately 0.5°C during the freshwater pulse and recovers approximately 50 yr after the freshwater pulse has ceased. The Morlet wavelet decomposition of the Niño-3.4 SST index (Fig. 9f) is characterized by two temporal periods of increased activity centered on 30 yr into the FWF and 40 yr after FWF input to the North Atlantic has ceased, respectively. One difference that is clearly evident, as compared to other studies that were involved in the recently published set of freshwater forcing experiments (e.g., Zhang and Delworth 2005; Dong and Sutton 2007; Timmermann et al. 2007), is that the increased ENSO activity is not constant but is manifested only during what appears to be a transient reaction or adjustment process to the periods of rapid change in the freshwater forcing with a response time of approximately 20 yr. The nature of this adjustment process will be further discussed in what follows. This adjustment process is also observed in the 0.3-Sv experiment (not shown) but with a longer response time into and out of the forcing. In the 0.3-Sv case, the reduction in tropical Pacific SSTs is impacted most significantly 100 yr after the FWF has stopped, with the full recovery requiring an additional 200 yr after the FWF has stopped.

The standard deviation of the Niño-3.4 SST index increases from approximately 1.0 to 1.5 throughout the duration of the FWF simulation then returns to the control values approximately 100 yr after the FWF has stopped. The increase in standard deviation reflects the general increase in amplitude of ENSO. The skewness of the time series is a measure often used to describe the asymmetry in strength between the positive El Niño events and negative La Niña events. The model control simulation before the onset of the FWF event is negatively skewed and indicates that there is a prevalence of stronger La Niña events before the FWF. During the onset of the increased ENSO power this prevalence weakens, a balance being reached between the relative strength of the positive and negative Niño-3.4 SST anomalies. The skewness of the observed Niño-3.4 index (Fig. 9a) is 0.4 and illustrates that El Niño events are on average stronger during the last 130 yr of observations. The opposite skewness (-0.33) in the control simulation may have implications for the results obtained in the FWF experiment. The skewness during the FWF event is approximately -0.1 and suggests that the El Niño events are becoming more prevalent but still not as prevalent as La Niña. Dong and Sutton (2007) find a similar behavior in their analysis of a FWF experiment and note that stronger El Niño events are characteristic of stronger ENSO variability, a result that is consistent with the last few decades of the observed ENSO cycle, which indicates the same relationship between stronger El Niños and increased variability (e.g., An and Jin 2004).

During Heinrich events or glacial stadial events, the ITCZ moves southward mainly in response to the increased meridional temperature gradient in the Northern Hemisphere. There is some evidence for an equivalent migration of the ITCZ during the YD in data taken from the coast of Brazil (Jennerjahn et al. 2004), which suggests a southward shift of the winter ITCZ of approximately 10° latitude with a more moderate shift of approximately 3° latitude of the summer ITCZ. The data also indicate increased humidity and precipitation in tropical South America due to enhanced northeasterly trade winds with the southward displacement of the ITCZ. Other proxy records indicative of east and west Pacific zonal SST gradients suggest that the position of the ITCZ is an important factor in the low-frequency modulation of ENSO (Koutavas et al. 2006) through the increase or decrease of southeasterly trade winds in the eastern tropical Pacific that enhance equatorial upwelling during late summer (Deser and Wallace 1990; Mitchell and Wallace 1992).

The model-predicted seasonal tropical precipitation and wind stress from 30°S to 30°N centered over the central Pacific and averaged over the 100 yr preceding the start of the FWF event (Fig. 10) illustrate the general position of the ITCZ. The corresponding precipitation and wind stress anomalies between climatology and the average of the last 50 yr of the FWF event (Fig. 10b) provide an indication of the evolution of the ITCZ

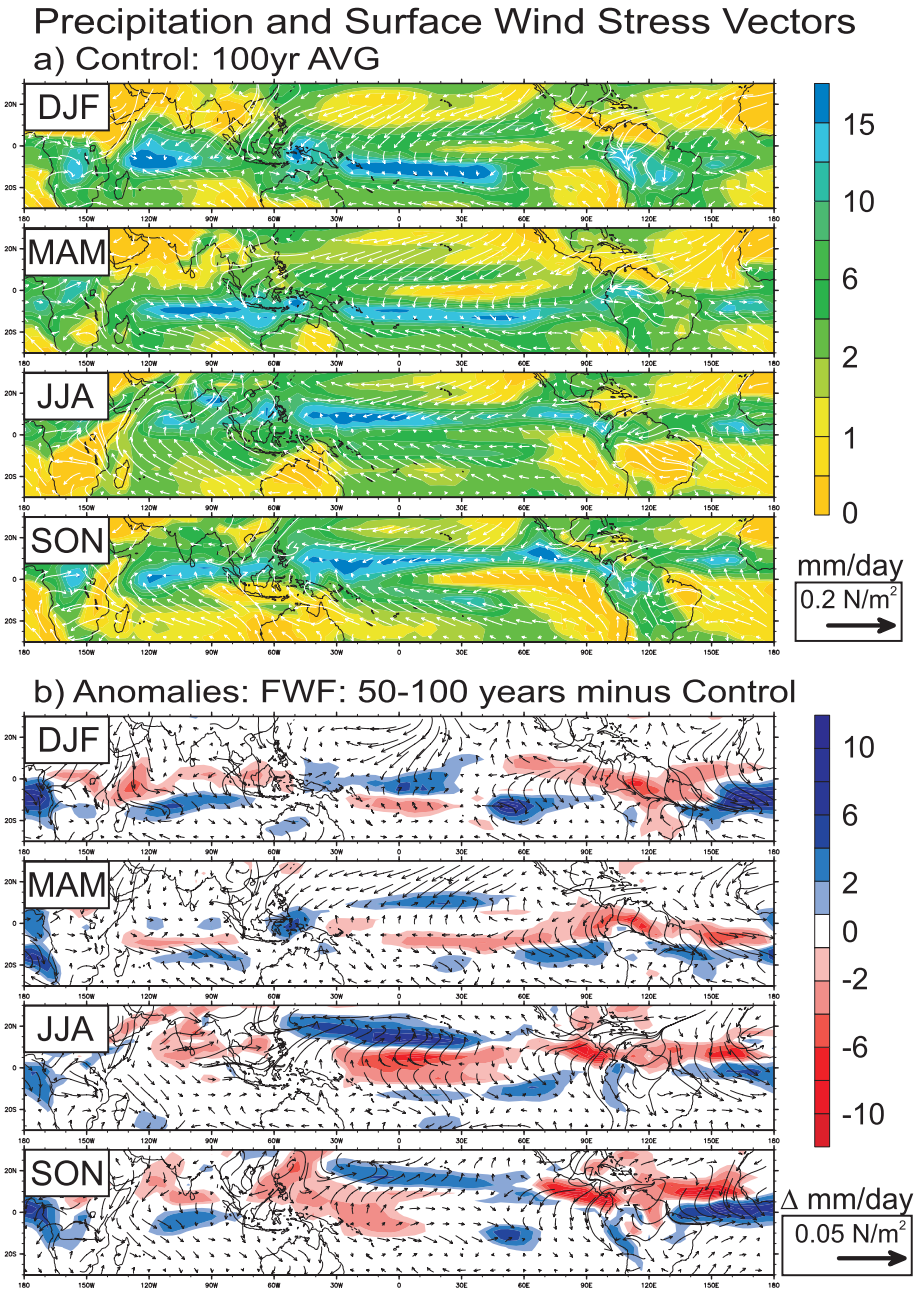

FIG. 10. Seasonal tropical total precipitation and surface wind stresses from 30°S to 30°N. (a) The 100-yr control average and (b) the difference between the average of years 50–100 during the freshwater forcing event minus the 100-yr control average. Seasonal averages are for DJF, March–May (MAM), JJA, and SON.

through the FWF event. The main feature in the tropical precipitation pattern is the maximum band of precipitation in the tropics that moves between summer hemispheres through the annual cycle. A double-ITCZ structure in this control simulation (Fig. 10a) causes excessive precipitation in the tropics and overly strong trade winds and is a common problem in many AOGCMs (Lin 2007). In the control simulation, the winter southern Pacific convergence zone (SPCZ) extends too far east into the tropical Pacific and is more intense in this region as well as over the southern tropical landmasses, as compared with observations from Xie and Arkin

(1996; not shown). In summer, the Pacific ITCZ is much too intense north of the equator and is characterized by an additional prominent band of precipitation south of the equator when compared with observations. A further difference from observations is the fact that the average observed position of the eastern tropical Pacific ITCZ resides north of the equator throughout the annual cycle. The Peruvian Andes and the subtropical South Pacific anticyclone in this region are responsible for the majority of this asymmetry (Philander et al. 1996; Takahashi and Battisti 2007). The impact of changes in the nature and position of the ITCZ on ENSO dynamics occurs primarily through wind–evaporation–SST feedbacks (WES). In the model, the northeasterlies are too strong in the western Pacific and the southeasterlies are too weak in the eastern Pacific in both winter and summer as compared with observations (Simmons and Gibson 2000). Other theories have described the interaction between the ITCZ and ENSO in terms of a modification of the meridional mode in the Atlantic and Pacific (e.g., see Chang et al. 2007 and references therein).

The average precipitation during the final 50 yr of the FWF event is characterized by a shift in the ITCZ toward the Southern Hemisphere. This shift is clearly evident in the magnitude of the precipitation anomalies, which are of the same magnitude as the ITCZ control values. The tropical ITCZ shifts south everywhere except in the central and western Pacific (Fig. 10b), which is mainly because the SPCZ is reduced in the west and enhanced in the east throughout the annual cycle. In summer, there is anomalously low precipitation over the equatorial central and western Pacific, leading to anomalous divergence of the wind. This is also observed in the wind stress anomaly pattern in this region, mainly during JJA, which suggests that there should be anomalous upwelling during winter in the central and western tropical Pacific. Along the coast of Peru in the southeastern tropical Pacific there are anomalous northerly winds, which may weaken the upwelling in the eastern Pacific. The zonally averaged Hadley cell (not shown) weakens by about 17% (intensifies by about 7%) in boreal summer (winter).

The modification of the tropical annual cycle through the FWF event is represented with a 20-yr running mean of the Niño-3.4 SST anomalies overlain upon the 20-yr running mean Niño-3.4 wind stress vector anomalies (Fig. 11a). These anomalies, positive (negative) in summer (winter), in the 100 yr prior to the onset of FWF pulse are constructed on the basis of averaging 200 yr of control and 500 yr of the FWF experiment annual cycle. It is immediately apparent that a significant distortion of the annual cycle begins to occur approximately 20 yr into the FWF event and is correlated with anomalous mean westerly wind stresses in the Niño-3.4 region. In DJF the opposite occurs, with a warming anomaly but of about half the magnitude of the JJA cooling (Fig. 11b). It is interesting to note that the warming is delayed with respect to the onset of the FWF event and does not reach a maximum until approximately 80 yr into the FWF event. This temporal asymmetry reinforces the notion that the JJA cooling originates in the Northern Hemisphere while the DJF warming originates in the Southern Hemisphere; a Northern Hemisphere–Southern Hemisphere ''seesaw effect.'' The temporal evolution of the tropical Pacific January SSTs through the FWF event (Fig. 11b) are a result of a Southern Hemisphere counterpart of the meridional ocean–atmosphere–ocean teleconnection described previously.

The 3–7-yr normalized band variance for the Niño-3.4 SSTs displayed together with the January and July Niño-3.4 SST time series through the FWF event (Fig. 11b) is extracted from the wavelet power spectrum analysis displayed in Fig. 9f. There is a strong correlation between the power in this band and the maximum change in SSTs in JJA during the onset of the FWF event and the return to equilibrium after the FWF has ceased. It is also striking that the ENSO activity becomes quiescent halfway through the FWF event and then becomes active again once the FWF event ends. The January warming does not appear to affect the ENSO variance to the same degree as the June cooling. A number of studies (e.g., Chang et al. 1995) have demonstrated a connection between the weakening of the tropical annual cycle and an enhancement and modification to the behavior of the ENSO phenomena. Chang et al. (1995) have also described a ''frequency entrainment'' mechanism, which involves the phase locking of ENSO to the annual cycle. Thus it is not surprising to find ENSO adjustment into and out of the FWF event, but it remains unclear what specific mechanisms are responsible for the adjustment behavior.

The equatorial Pacific annual cycle of SST variations at 4°N, the equator, and 4°S for the observations, the control experiment, and the anomaly between the last 20 yr of the FWF and the control may shed some light on mechanisms involved in ENSO adjustment (Fig. 12a). The observed SSTs, from the HadISST dataset (Rayner et al. 2003), have an annual cycle in the tropical Pacific that is fairly constant in the western Pacific but with a well-defined annual cycle in the eastern Pacific. The annual cycle in the eastern Pacific peaks in March and has a minimum in September. In the control experiment we see that the annual cycle in the tropical eastern Pacific is considerably different from that which is observed and has two maxima and

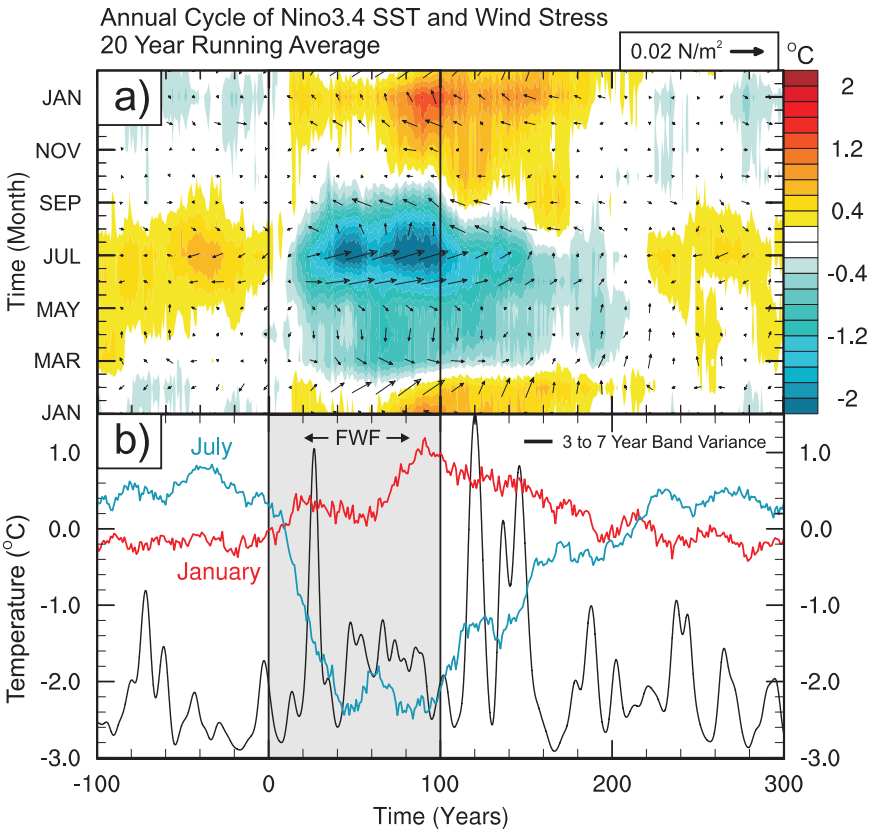

FIG. 11. (a) The time evolution of the 20-yr running mean annual cycle of the Niño-3.4 SSTA index and Niño-3.4 surface wind stress anomalies through the FWF experiment. (b) Comparison of the time series of the SST anomalies for January (red) and July (blue) with the Niño-3.4 SSTA 3–7-yr band power (black) from the Morel power spectrum in Fig. 9f. Wind stress vectors which point up and right in the figure are southwesterly wind stress anomalies (anomalies toward the north and east).

two minima during the year. Near the end of the FWF experiment, the annual cycle has reorganized and is characterized by a pattern of westward-propagating temperature anomalies with periods synchronous with the annual cycle, as expected. The asymmetry of the anomaly, stronger cooling in summer and weaker warming in winter (Fig. 12a), illustrates the impact of the ocean–atmosphere–ocean teleconnection in transporting the cool signal from the Northern Hemisphere and the warm signal from the Southern Hemisphere into the equatorial Pacific basin.

The depth of the 20°C isotherm, a reliable indicator of the thermocline depth in the tropical Pacific, exerts a strongly controlling influence upon ENSO dynamics (Fig. 12b). The observed 20°C isotherm depth in the tropics (Antonov et al. 1998; *World Ocean Atlas 1998*) is less variable than the control simulation mean thermocline depth. The control experiment has an equatorial Pacific mean thermocline that is also too shallow in both the western and eastern tropical Pacific, which may explain the excessively strong ENSO variability when compared with observations through an increase in air–sea coupling and the strength of the Bjerknes feedback (Bjerknes 1969). The anomalies in the mean thermocline depth in the last 20 yr of the FWF event are symmetric about the equator at 4°S and 4°N. The mean thermocline is deeper (shallower) when the SSTs are cooler (warmer) at 4°S and 4°N. The mean thermocline anomalies also propagate westward at 4°S and 4°N and eastward at the equator through the course of the annual cycle. In late summer, within this latitude band, the mean thermocline during the FWF event achieves a more ''La Niña–like'' (more sloping) thermocline (deeper in the west Pacific, shallower in the east Pacific) and a more ''El Niño–like'' (less sloping) thermocline in early spring. The two prevalent spatial and temporal anomalies in the mean thermocline are separated by 6 months. The thermocline depth anomalies appear to

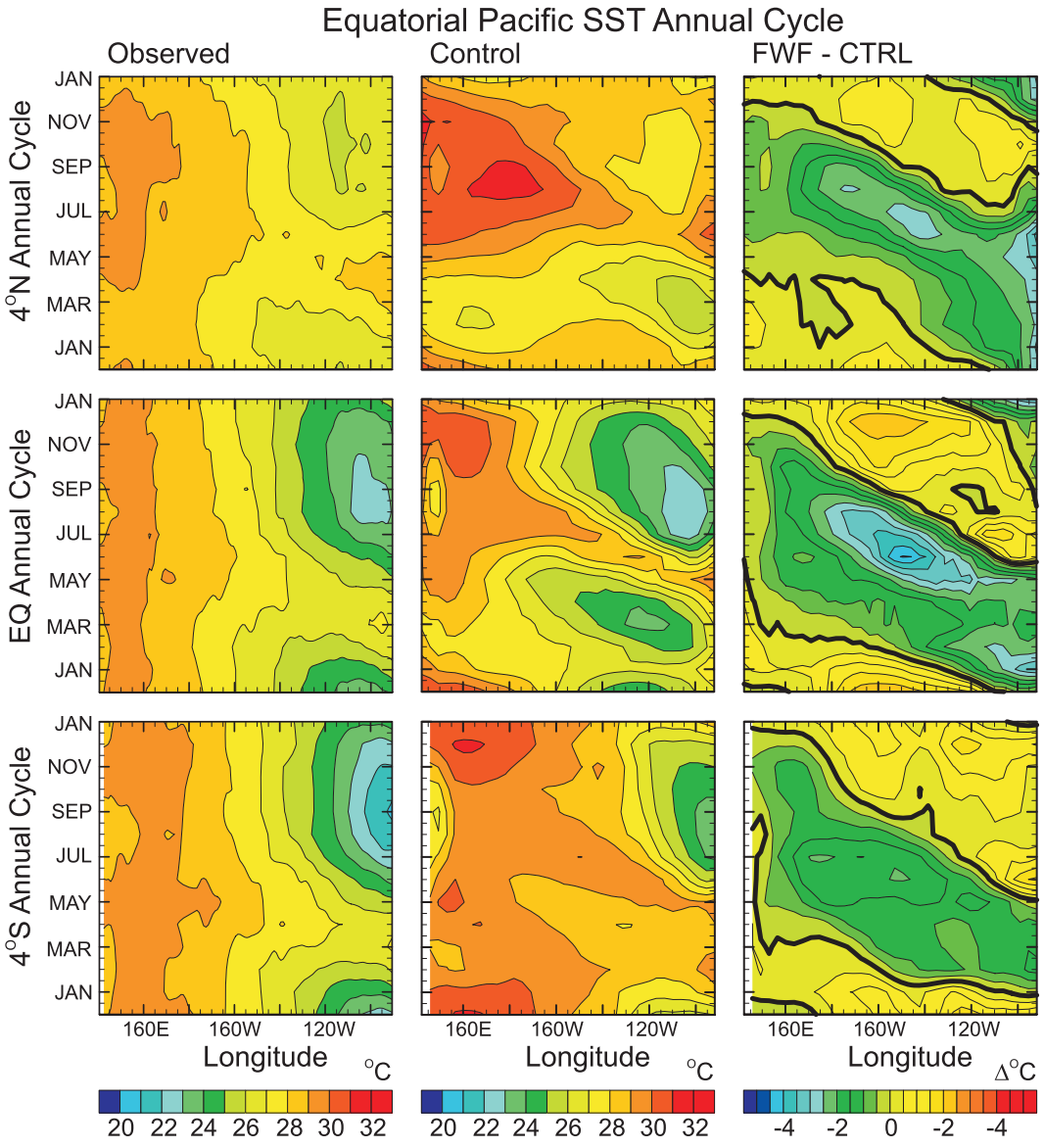

FIG. 12. (a) The cross-equatorial Pacific annual cycle at (top) 4°N, (middle) the equator, and (bottom) 4°S for (left) the observed (1870–present), (middle) the average control (200 yr before the freshwater forcing event), and (right) the difference between years 80–100 of the freshwater forcing event and the control. (b) As in (a), but for the depth of the 20°C isotherm.

be much more influenced by the changes in wave propagation than by the SST anomalies.

4. Summary and discussion

This study has examined the impact of a destabilization of polar climate associated with the addition of freshwater to the surface of the North Atlantic and the significant impact of this destabilization upon tropical climate variability. This forcing acts to reduce the AMOC through reductions in NADW formation until the Northern Hemisphere experiences a marked reduction in surface air temperature and a large expansion in Northern Hemisphere sea ice. Our preliminary results are based on an experiment in which a control climate is perturbed by the addition of 1.0 Sv of freshwater to the North Atlantic between 50° and 70°N for 100 yr and the system subsequently allowed to recover. The addition of a freshwater forcing of magnitude less than 0.3 Sv appears to be a threshold in this

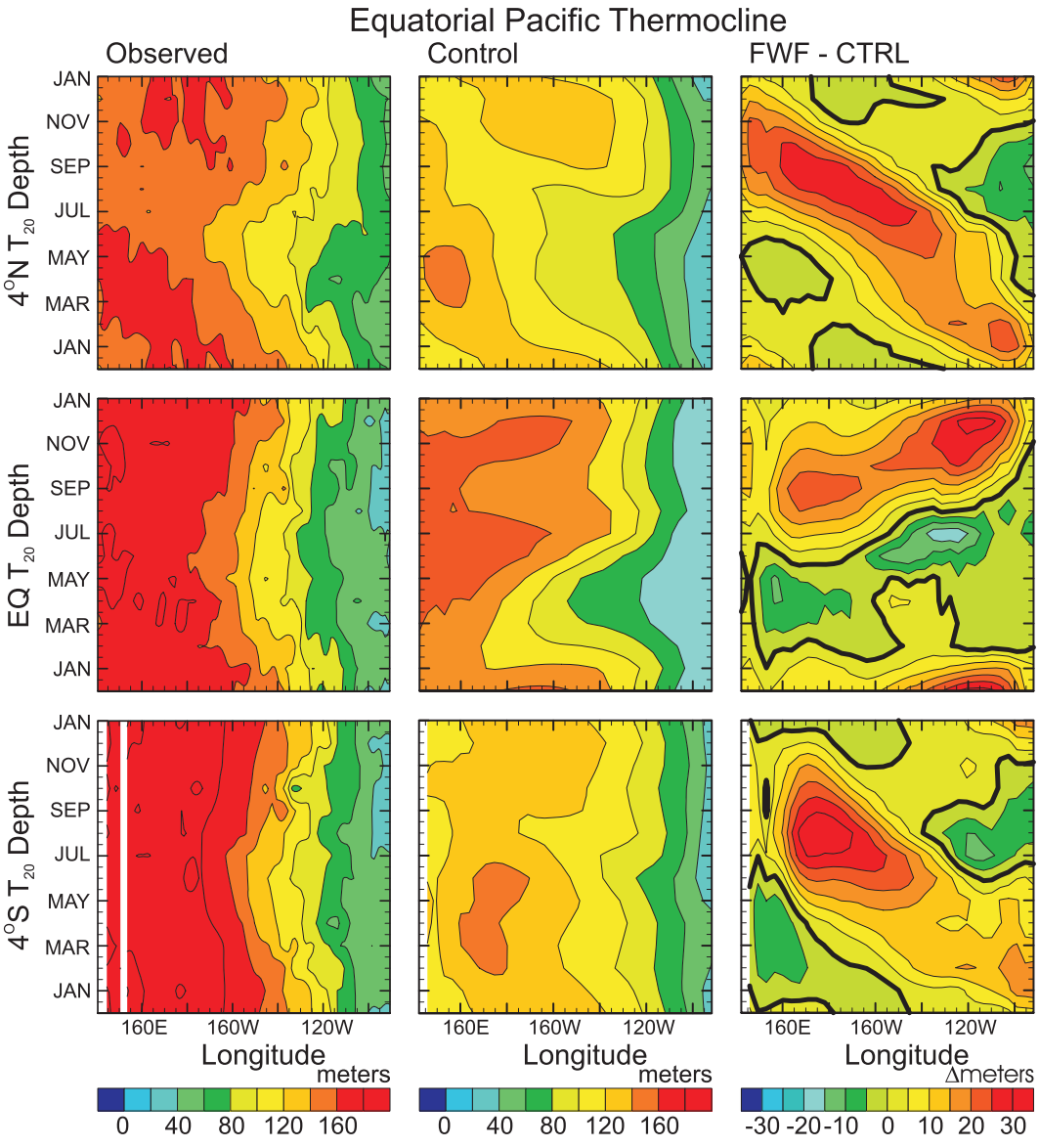

FIG. 12. (*Continued*)

model below which changes in surface temperature at high latitudes are not significantly impacted. Freshwater input of strength lower than 0.3 Sv delivers a surface temperature change that is much less than that inferred on the basis of the GISP2 ice core data for Greenland surface temperatures during the YD. The expansion in sea ice contributes in a highly significant way to surface temperature decrease and to the locations of the deep-water formation sites. After the freshwater input to the North Atlantic ceases, the renewal of deep-water formation initially develops in the high- and midlatitude Atlantic. An overturning cell organizes in the midlatitude central Atlantic approximately 100 yr after the forcing stops. The Gulf Stream never slows significantly during the entire period of the FWF experiment, suggesting that the revitalization of the overturning process is initiated by wind stress forcing and the associated midlatitude Ekman pumping. The reorganization of the AMOC only appears approximately 100 yr after the FWF event and plays a role in aiding the sea ice to recover to its normal (less extensive) position through the transport of warm saline waters to the surface of the North Atlantic.

The impact of the slowdown and recovery of the AMOC and the resulting high-latitude cooling eventually becomes evident in tropical Pacific variability but

with a time lag of approximately 20 yr. We have investigated two distinct coupled ocean–atmosphere–ocean ''bridges'' that impact changes observed in the simulation, namely:

1) An ocean–atmosphere–ocean ''bridge'' in which the initial transport of the high-latitude ocean temperature signal occurs by the advection of cool SSTs from the North Atlantic to the tropical Atlantic and Caribbean Sea by the mid-Atlantic ocean gyre. This oceanic signal is then transported into the tropical Pacific by the subtropical North Atlantic anticyclone and the northeasterly trade winds (e.g., see also Timmermann et al. 2007). The advection of cool JJA SSTs from the North Atlantic appears to amplify the strength of the northeasterly trades. These act so as to synchronously transmit the cooling signal to the eastern Pacific, and thus modify the annual cycle in boreal summer (JJA). The interhemispheric ''seesaw,'' which results from reduced transport of heat from the Southern to the Northern Hemisphere, results in a warmer Southern Hemisphere during and after the FWF event. This warming signal, weaker than the summer cooling, is transmitted to the eastern tropical Pacific during austral summer (DJF). The result is a weakening in the eastern tropical Pacific annual cycle consistent with the majority of studies that have investigated the impact of FWF on ENSO (Timmermann et al. 2007; Dong and Sutton 2007). The southeasterly trade winds play a role in transporting the warm Southern Hemisphere temperature anomaly into the eastern tropical Pacific during austral summer (DJF) that matures during the latter stages of the FWF event. The tropical Pacific warm anomaly in austral summer (DJF) may also be zonally advected throughout the South Pacific by mean Southern Hemisphere westerlies and the Antarctic Circumpolar Current. A clear connection has also been demonstrated between the Atlantic and Pacific Walker circulations during the FWF event, both at upper and lower levels. The Pacific Walker cell responds in a seasonally asymmetric manner during the freshwater forcing. The Walker cell appears to move westward during DJF and eastward during JJA. The respective seasonal shifts result in westerly wind anomalies in the western Pacific in JJA and may impact the strength of ENSO during this adjustment.
2) An ocean–atmosphere–ocean ''bridge'' in which the Northern Hemisphere cooling that is experienced during the reduction in AMOC is zonally propagated across the Northern Hemisphere through the action of the westerlies and by anomalous stationary planetary wave forcing in boreal winter (DJF). This forcing increases the strength of both the Aleutian and Icelandic lows in winter and may be involved in explaining the high temporal correlation between Greenland proxy temperature records and upwelling productivity records from the Santa Barbara Basin. The increase in the Aleutian low and subsequent surface ocean thermal forcing during winter in the northeastern Pacific was also investigated as a possible oceanic pathway to the tropical Pacific. The negative temperature anomaly that is imprinted into the northeastern Pacific Ocean during the FWF event does not appear to propagate into the tropical Pacific. We cannot, however, rule out the possibility that this teleconnection could impact tropical Pacific interdecadal variability through an ocean basin adjustment process in which midlatitude Pacific oceanic Rossby waves and west Pacific midlatitude coastal Kelvin waves redistribute thermal anomalies from this source region into the western tropical Pacific. The teleconnection that operates in the meridional direction impacts SSTs in the tropical Atlantic and Pacific with a delay of approximately 20 yr and correlates precisely with changes in the bursts of ENSO activity. The zonal teleconnection between the North Atlantic and the North Pacific is almost instantaneous and would thus require a Pacific oceanic teleconnection between the midlatitudes and tropics to operate on the same 20-yr time scale. This study did not find such a mechanism that might provide an alternate explanation for the bursts in ENSO power 20 yr after the initial input of freshwater to the North Atlantic.

Changes to the mean structure of the ocean and atmosphere in the tropical and extratropical Pacific during the FWF event are especially important in modifying ENSO dynamics. The dominant response in ENSO activity occurs at the onset and cessation of the FWF event. The tropical atmosphere responds with a southward shift of the ITCZ in both the tropical eastern Pacific and tropical Atlantic that occurs approximately 20 yr after the FWF input to the North Atlantic begins. The cross-equatorial northeasterly winds that advect cold anomalies from the North Atlantic to the east Pacific also help establish the mean position of the ITCZ in the tropical eastern Pacific.

It was demonstrated that the anomalous ENSO power appeared to result from changes in the mean tropical Pacific annual cycle in boreal summer. These changes consisted of anomalous cooling and anomalous westerly wind stress, consistent with the eastward Walker cell shift. Warming anomalies in boreal winter, along with

anomalous easterly wind stress, are also significant but of half the magnitude of boreal summer changes. The latter changes are consistent with the westward shift of the Walker cell during DJF and may also play a role in influencing ENSO dynamics, but to a lesser degree. The nonlinear interaction between the natural modes of ENSO oscillation, which span a broad range of periods, and the modulation of the tropical annual cycle illustrate the subtle influence of frequency entrainment in this nonlinear system.

Acknowledgments. This work is supported by the Canadian Foundation for Climate and Atmospheric Sciences (CFCAS) and the Natural Sciences and Engineering Research Council of Canada through Discovery Grant A9627. This paper is a contribution to the Polar Climate Stability Network, which is funded by CFCAS and a consortium of Canadian universities. We also thank the anonymous reviewers for useful suggestions.

REFERENCES

Alley, R. B., and Coauthors, 1993: Abrupt increase in Greenland snow accumulation at the end of the Younger Dryas. *Nature,* **362,** 527–529.

An, S.-I., and F.-F. Jin, 2004: Nonlinearity and asymmetry of ENSO. *J. Climate,* **17,** 2399–2412.

Antonov, J., S. Levitus, T. P. Boyer, M. E. Conkright, T. O'Brien, and C. Stephens, 1998: *Atlantic Ocean Temperature Fields*. Vol. 1, *World Ocean Atlas 1998,* NOAA Atlas NESDIS 27, 166 pp. [Available online at http://www.cdc.noaa.gov/.]

Applegate, P. J., T. V. Lowell, and R. B. Alley, 2008: Comment on ''Absence of cooling in New Zealand and the adjacent ocean during the Younger Dryas chronozone.'' *Science,* **320,** 746d.

Barrows, T. T., S. J. Lehman, L. K. Fifield, and P. De Deckker, 2007: Absence of cooling in New Zealand and the adjacent ocean during the Younger Dryas chronozone. *Science,* **318,** 86–89.

Bitz, C. M., J. C. H. Chiang, W. Cheng, and J. J. Barsugli, 2007: Rates of thermohaline recovery from freshwater pulses in modern, Last Glacial Maximum, and greenhouse warming climates. *Geophys. Res. Lett.,* **34,** L07708, doi:10.1029/2006GL029237.

Bjerknes, J., 1969: Atmospheric teleconnections from the equatorial Pacific. *Mon. Wea. Rev.,* **97,** 163–172.

Boville, B. A., and P. R. Gent, 1998: The NCAR Climate System Model, version one. *J. Climate,* **11,** 1115–1130.

——, J. T. Kiehl, P. J. Rasch, and F. O. Bryan, 2001: Improvements to the NCAR CSM-1 for transient climate simulations. *J. Climate,* **14,** 164–179.

Broecker, W. S., 1991: The great ocean conveyor. *Oceanography,* **4,** 79–89.

——, 1998: Paleocean circulation during the last deglaciation: A bipolar seesaw? *Paleoceanography,* **13,** 119–121.

——, J. P. Kennett, B. P. Flower, J. T. Teller, S. Trumbore, G. Bonani, and W. Wolfli, 1989: Routing of meltwater from the Laurentide Ice Sheet during the Younger Dryas cold episode. *Nature,* **341,** 318–321.

Bush, A. B. G., 2003: Baroclinic waves in climates of the Earth's past. *Nonlinear Processes in Geophysical Fluid Dynamics,* O. U. Velasco-Fuentes et al., Eds., Kluwer Academic Publishers, 127–139.

Chang, P., L. Ji, B. Wang, and T. Li, 1995: Interactions between the seasonal cycle and El Niño–Southern Oscillation in an intermediate coupled ocean–atmosphere model. *J. Atmos. Sci.,* **52,** 2353–2372.

——, L. Zhang, R. Saravanan, D. J. Vimont, J. C. H. Chiang, L. Ji, H. Seidel, and M. K. Tippett, 2007: Pacific meridional mode and El Niño–Southern Oscillation. *Geophys. Res. Lett.,* **34,** L16608, doi:10.1029/2007GL030302.

Chiang, J. C. H., and D. J. Vimont, 2004: Analogous Pacific and Atlantic meridional modes of tropical atmosphere–ocean variability. *J. Climate,* **17,** 4143–4157.

Deser, C., and J. M. Wallace, 1990: Large-scale atmospheric circulation features of warm and cold episodes in the tropical Pacific. *J. Climate,* **3,** 1254–1281.

——, M. A. Alexander, and M. S. Timlin, 1996: Upper-ocean thermal variations in the North Pacific during 1970–1991. *J. Climate,* **9,** 1840–1855.

Dong, B., and R. T. Sutton, 2007: Enhancement of ENSO variability by a weakened Atlantic thermohaline circulation in a coupled GCM. *J. Climate,* **20,** 4920–4939.

——, ——, and A. A. Scaife, 2006: Multidecadal modulation of El Niño–Southern Oscillation (ENSO) variance by Atlantic Ocean sea surface temperatures. *Geophys. Res. Lett.,* **33,** L08705, doi:10.1029/2006GL025766.

d'Orgeville, M., and W. R. Peltier, 2007: On the Pacific Decadal Oscillation and the Atlantic Multidecadal Oscillation: Might they be related? *Geophys. Res. Lett.,* **34,** L23705, doi:10.1029/2007GL031584.

EPICA Community Members, and Coauthors, 2006: One-to-one coupling of glacial climate variability in Greenland and Antarctica. *Nature,* **444,** 195–198.

Fedorov, A. V., and S. G. Philander, 2000: Is El Niño changing? *Science,* **288,** 1997–2002.

Flato, G. M., and W. D. Hibler III, 1992: Modeling pack ice as a cavitating fluid. *J. Phys. Oceanogr.,* **22,** 626–651.

Gent, P. R., F. O. Bryan, G. Danabasoglu, S. C. Doney, W. R. Holland, W. G. Large, and J. C. McWilliams, 1998: The NCAR Climate System Model global ocean component. *J. Climate,* **11,** 1287–1306.

Gill, A. E., 1980: Some simple solutions for heat-induced tropical circulation. *Quart. J. Roy. Meteor. Soc.,* **106,** 447–462.

Grachev, A. M., and J. P. Severinghaus, 2005: A revised +10 +/−4°C magnitude of the abrupt change in Greenland temperature at the Younger Dryas termination using published GISP2 gas isotope data and air thermal diffusion constants. *Quat. Sci. Rev.,* **24,** 513–519.

Gu, D., and S. G. H. Philander, 1997: Interdecadal climate fluctuations that depend on exchanges between the tropics and extratropics. *Science,* **275,** 805–807.

Guilyardi, E., 2006: El Niño–mean state–seasonal cycle interactions in a multi-model ensemble. *Climate Dyn.,* **26,** 329–348.

Hendy, I. L., J. P. Kennett, E. B. Roark, and B. L. Ingram, 2002: Apparent synchroneity of submillennial scale climate events between Greenland and Santa Barbara Basin, California from 30–10 ka. *Quat. Sci. Rev.,* **21,** 1167–1184.

——, T. F. Pedersen, J. P. Kennett, and R. Tada, 2004: Intermittent existence of a southern Californian upwelling cell during

submillennial climate change of the last 60 kyr. *Paleoceanography,* **19,** PA3007, doi:10.1029/2003PA000965.

Hu, A., G. A. Meehl, and W. Han, 2007: Role of the Bering Strait in the thermohaline circulation and abrupt climate change. *Geophys. Res. Lett.,* **34,** L05704, doi:10.1029/2006GL028906.

Jennerjahn, T. C., V. Ittekkot, H. W. Arz, H. Behling, J. Patzold, and G. Wefer, 2004: Asynchronous terrestrial and marine signals of climate change during Heinrich events. *Science,* **306,** 2237–2239.

Kiehl, J. T., J. J. Hack, G. B. Bonan, B. A. Boville, D. L. Williamson, and P. J. Rasch, 1998: The National Center for Atmospheric Research Community Climate Model: CCM3. *J. Climate,* **11,** 1131–1149.

Kienast, M., S. S. Kienast, S. E. Calvert, T. I. Eglinton, G. Mollenhauer, R. Francois, and A. C. Mix, 2006: Eastern Pacific cooling and Atlantic overturning circulation during the last deglaciation. *Nature,* **443,** 846–849.

Koutavas, A., J. Lynch-Stieglitz, T. M. Marchitto, and J. P. Sachset, 2002: El Niño-like pattern in ice age tropical Pacific sea surface temperature. *Science,* **297,** 226–230.

——, P. B. deMenocal, G. C. Olive, and J. Lynch-Stieglitz, 2006: Mid-Holocene El Niño–Southern Oscillation (ENSO) attenuation revealed by individual foraminifera in eastern tropical Pacific sediments. *Geology,* **34,** 993–996.

Krebs, U., and A. Timmermann, 2007: Tropical air–sea interactions accelerate the recovery of the Atlantic Meridional Overturning Circulation after a major shutdown. *J. Climate,* **20,** 4940–4956.

Lin, J.-L., 2007: The double-ITCZ problem in IPCC AR4 coupled GCMs: Ocean–atmosphere feedback analysis. *J. Climate,* **20,** 4497–4525.

Liu, Z., and M. Alexander, 2007: Atmospheric bridge, oceanic tunnel, and global climatic teleconnections. *Rev. Geophys.,* **45,** 1–34.

Lowell, T., and Coauthors, 2005: Testing the Lake Agassiz meltwater trigger for the Younger Dryas. *Eos, Trans. Amer. Geophys. Union,* **86,** doi:10.1029/2005EO400001.

Manabe, S., and R. J. Stouffer, 1988: Two stable equilibria of a coupled ocean–atmosphere model. *J. Climate,* **1,** 841–866.

——, and ——, 1997: Coupled ocean–atmosphere model response to freshwater input: Comparison to Younger Dryas event. *Paleoceanography,* **12,** 321–336.

McManus, J. F., R. Francois, J. M. Gherardi, L. D. Keigwin, and S. Brown-Leger, Collapse and rapid resumption of Atlantic meridional circulation linked to deglacial climate changes. *Nature,* **428,** 834–837.

McPhaden, M. J., S. E. Zebiak, and M. H. Glantz, 2006: ENSO as an integrating concept in earth science. *Science,* **314,** 1740–1745.

Mitchell, T. P., and J. M. Wallace, 1992: The annual cycle in equatorial convection and sea surface temperature. *J. Climate,* **5,** 1140–1156.

Moy, C. M., G. O. Seltzer, D. T. Rodbell, and D. M. Anderson, 2002: Variability of El Niño/Southern Oscillation activity at millennial timescales during the Holocene epoch. *Nature,* **420,** 162–165.

Okumura, Y. M., C. Deser, A. Hu, A. Timmermann, and S.-P. Xie, 2009: North Pacific climate response to freshwater forcing in the subarctic North Atlantic: Oceanic and atmospheric pathways. *J. Climate,* **22,** 1424–1445.

Otto-Bliesner, B. L., 1999: El Niño/La Niña and Sahel precipitation during the middle Holocene. *Geophys. Res. Lett.,* **26,** 87–90.

——, and E. C. Brady, 2001: Tropical Pacific variability in the NCAR Climate System Model. *J. Climate,* **14,** 3587–3607.

Pahnke, K., J. P. Sachs, L. Keigwin, A. Timmermann, and S.-P. Xie, 2007: Eastern tropical Pacific hydrologic changes during the past 27,000 years from D/H ratios in alkenones. *Paleoceanography,* **22,** PA4214, doi:10.1029/2007PA001468.

Peltier, W. R., 2007: Rapid climate change and Arctic Ocean freshening. *Geology,* **35,** 1147–1148.

——, and L. P. Solheim, 2004: The climate of the Earth at Last Glacial Maximum: Statistical equilibrium state and a mode of internal variability. *Quat. Sci. Rev.,* **23,** 335–357.

——, G. Vettoretti, and M. Stastna, 2006: Atlantic meridional overturning and climate response to Arctic Ocean freshening. *Geophys. Res. Lett.,* **33,** L06713, doi:10.1029/2005GL025251.

Philander, S. G. H., D. Gu, D. Halpern, G. Lambert, N.-C. Lau, T. Li, and R. C. Pacanowski, Why the ITCZ is mostly north of the equator. *J. Climate,* **9,** 2958–2972.

Rayner, N. A., D. E. Parker, E. B. Horton, C. K. Folland, L. V. Alexander, D. P. Rowell, E. C. Kent, and A. Kaplan, 2003: Global analyses of sea surface temperature, sea ice, and night marine air temperature since the late nineteenth century. *J. Geophys. Res.,* **108** (D14), 4407, doi:10.1029/2002JD002670.

Rein, B., A. Lückge, L. Reinhardt, F. Sirocko, A. Wolf, and W.-C. Dullo, 2005: El Niño variability off Peru during the last 20,000 years. *Paleoceanography,* **20,** PA4003, doi:10.1029/2004PA001099.

Rodbell, D. T., G. O. Seltzer, D. M. Anderson, M. B. Abbot, D. B. Enfield, and J. H. Newman, 1999: An ~15,000-year record of El Niño driven alleviation in southwestern Ecuador. *Science,* **283,** 516–520.

Rosenthal, T., and A. J. Broccoli, 2004: In search of paleo-ENSO. *Science,* **304,** 219–221.

Semtner, A. J., 1976: A model for the thermodynamic growth of sea ice in numerical investigations of climate. *J. Phys. Oceanogr.,* **6,** 379–389.

Shulmeister, J., D. T. Rodbell, M. K. Gagan, and G. O. Seltzer, 2006: Inter-hemispheric linkages in climate change: Paleo-perspectives for future climate change. *Climate Past,* **2,** 167–185.

Simmons, A. J., and J. K. Gibson, 2000: The ERA-40 project plan. ERA-40 Project Rep. Series No.1, ECMWF, Reading, United Kingdom, 63 pp.

Stocker, T. F., 1998: The seesaw effect. *Science,* **282,** 61–62.

——, A. Timmermann, M. Renold, and O. Timm, 2007: Effects of salt compensation on the climate model response in simulations of large changes of the Atlantic meridional overturning circulation. *J. Climate,* **20,** 5912–5928.

Stommel, H. M., 1961: Thermohaline convection with two stable regimes of flow. *Tellus,* **13,** 224–230.

Stouffer, R. J., and Coauthors, 2006: Investigating the causes of the response of the thermohaline circulation to past and future climate changes. *J. Climate,* **19,** 1365–1387.

Takahashi, K., and D. S. Battisti, 2007: Processes controlling the mean tropical pacific precipitation pattern. Part I: The Andes and the eastern Pacific ITCZ. *J. Climate,* **20,** 3434–3451.

Tarasov, L., and W. R. Peltier, 2005: Arctic freshwater forcing of the Younger Dryas cold reversal. *Nature,* **435,** 662–666.

Timmermann, A., S.-I. An, U. Krebs, and H. Goosse, 2005: ENSO suppression due to weakening of the North Atlantic thermohaline circulation. *J. Climate,* **18,** 3122–3139.

——, and Coauthors, 2007: The influence of a weakening of the Atlantic meridional overturning circulation on ENSO. *J. Climate,* **20,** 4899–4919.

Torrence, C., and G. P. Compo, 1998: A practical guide to wavelet analysis. *Bull. Amer. Meteor. Soc.,* **79,** 61–78.

Wang, C., 2002: Atmospheric circulation cells associated with the El Niño–Southern Oscillation. *J. Climate,* **15,** 399–419.

Weatherly, J. W., B. P. Briegleb, W. G. Large, and J. A. Maslanik, 1998: Sea ice and polar climate in the NCAR CSM. *J. Climate,* **11,** 1472–1486.

Wu, L., W. Li, C. Yang, and S.-P. Xie, 2008: Global teleconnections in response to a shutdown of the Atlantic Meridional Overturning Circulation. *J. Climate,* **21,** 3002–3019.

Wu, X., L. Deng, X. Song, G. Vettoretti, W. R. Peltier, and G. J. Zhang, 2007: Impact of a modified convective scheme on the Madden–Julian Oscillation and El Niño–Southern Oscillation in a coupled climate model. *Geophys. Res. Lett.,* **34,** L16823, doi:10.1029/2007GL030637.

Xie, P., and P. A. Arkin, 1996: Analyses of global monthly precipitation using gauge observations, satellite estimates, and numerical model predictions. *J. Climate,* **9,** 840–858.

Zhang, R., and T. L. Delworth, 2005: Simulated tropical response to a substantial weakening of the Atlantic thermohaline circulation. *J. Climate,* **18,** 1853–1860.

——, and ——, 2007: Impact of the Atlantic Multidecadal Oscillation on North Pacific climate variability. *Geophys. Res. Lett.,* **34,** L23708, doi:10.1029/2007GL031601.